energies

MDPI

Article

Numerical Analysis of Altered Parallel Flow Heat Exchanger with Promoted Geometry at Multifarious Baffle Prolongs

Mehmet Akif Kartal [1,*] and Ahmet Feyzioğlu [2]

[1] Distance Education Application and Research Center, Bandırma Onyedi Eylül University, 10200 Bandırma, Turkey
[2] Mechanical Engineering, Production Planning and Control Department, Technology Faculty, Marmara University, 34722 Kadıköy, Turkey; ahmet.feyzioglu@marmara.edu.tr
* Correspondence: mkartal@bandirma.edu.tr

Abstract: This study investigated the influence of BFFSP on the thermohydraulic performance of a SATHEC(s) using a novel computational approach. The novelty lies in the detailed exploration of the interplay between BFFSP, MFRT, and key performance parameters. Unlike prior studies, which often focus on a limited range of operating conditions, this work employs a comprehensive parametric analysis encompassing two BFFSPs (95 mm and 125 mm) and four MFRTs (0.1, 0.3, 0.5, and 0.7 kg/h). This extensive analysis provides a deeper understanding of the trade-off between the HTRFR enhancement and PDP associated with the BFFSP across a wider range of operating conditions. This investigation leverages the power of computational fluid dynamics (CFD) simulations for high-fidelity analysis. ANSYS Fluent, a widely recognized commercial CFD software package, was used as a computational platform. A three-dimensional steady-state model of HEXR geometry was established. The cold fluid was modeled as water, and the hot fluid was modeled as water. The selection of appropriate turbulence models is crucial for accurate flow simulations within the complex geometry of HEXR. This study incorporates a well-established two-equation turbulence model to effectively capture turbulent flow behavior. The governing equations for mass, momentum, and energy conservation were solved numerically within the CFD framework. Convergence criteria were meticulously established to ensure the accuracy and reliability of the simulation results. BFFs are crucial components in HEXRs as they promote fluid mixing and turbulence on the HTRFR surface, thereby enhancing HTRFR. This study explores the interplay between BFFSP and HTRFR effectiveness. It is hypothesized that a larger BFFSP (125 mm) might lead to a higher HTC owing to the increased fluid mixing. However, the potential drawbacks of the increased PDP due to the flow restriction also need to be considered. The PDP across the HEXR is a critical parameter that affects pumping costs and overall system yield. This study investigates the impact of BFFSP on the PDP. It is expected that a larger BFFSP (125 mm) will result in a higher PDP, owing to the increased resistance to fluid flow. Here, we aim to quantify the trade-off between enhanced HTRFR and increased PDP associated with different BFFSPs. The optimal design of an HEXR seeks a balance between achieving a high HTRFR rate and minimizing pressure losses. HTRPD, a metric combining both HTC and PDP, was employed to evaluate the thermohydraulic performance. We hypothesized that a specific BFFSP might offer a superior HTRPD, indicating an optimal balance between HTRFR effectiveness and PDP for the investigated HEXR geometry and operating conditions. CFD simulations were conducted using ANSYS Fluent to analyze the effects of BFFSP and MFRT on the HTC, PDP, and HTRPD. The simulations employed a commercially available HEXR geometry with water as the cold and hot fluid. The results are presented and discussed to elucidate the relationships between the BFFSP, MFRT, and key performance parameters of the HEXR. This study provides valuable insights into the influence of BFFSP on the thermohydraulic performance of HEXRs. The findings can aid in optimizing the HEXR design by identifying the BFFSP that offers the best compromise between HTRFR enhancement and PDP for specific operating conditions. The results contribute to the knowledge base of HEXR design and optimization, potentially leading to improved yield in various industrial applications. The results indicate that a larger BFFSP (125 mm) leads to higher outlet temperatures but also results in a higher PDP compared to the 95 mm design. Conversely, the 95 mm BFFSP exhibits a lower PDP but

check for updates

Citation: Kartal, M.A.; Feyzioğlu, A. Numerical Analysis of Altered Parallel Flow Heat Exchanger with Promoted Geometry at Multifarious Baffle Prolongs. *Energies* **2024**, *17*, 1676. https://doi.org/10.3390/en17071676

Academic Editors: Tadeusz Bohdal and Artur Blaszczuk

Received: 5 March 2024
Revised: 25 March 2024
Accepted: 28 March 2024
Published: 1 April 2024

Copyright: © 2024 by the authors. Licensee MDPI, Basel, Switzerland. This article is an open access article distributed under the terms and conditions of the Creative Commons Attribution (CC BY) license (https://creativecommons.org/licenses/by/4.0/).

achieves a lower HTC. In terms of thermohydraulic performance, as indicated by HTRPD, the 95 mm BFFSP with the lowest MFRT (0.1 kg/h) achieved the highest value, surpassing the 125 mm design by 19.81%. This suggests that a 95 mm BFFSP offers a better trade-off between HTRFR effectiveness and pressure loss, potentially improving the overall HEXR performance.

Keywords: pressure drop; exchanger; CFD; baffle gap; HTRFR; flow rate; turbulence; heat coefficient; thermohydraulic performance

1. Introduction

Parallel flow HEXR(s) are a type of HEXR in which hot and cold fluids flow in the same direction. These types of HEXRs are widely used due to their simple design and ease of manufacturing. In terms of parallel flow HEXR techniques, there are three types of exchangers: single-tube, double-tube, and multi-tube HEXRs. A single-tube HEXR is the simplest type of parallel-flow HEXR. Inside a single tube, the hot and cold fluids flow in opposite directions. Due to their low HTRFR capacity, these types of HEXRs are typically used in small-scale applications. Double-tube HEXR: in this type of HEXR, two tubes are placed, one inside the other. Hot and cold fluids flow in opposite directions through the inside and outside of the tubes. Compared to single-tube HEXRs, these types of HEXRs have a higher HTRFR capacity. Multi-tube HEXR: in this type of HEXR, multiple tubes are placed inside a shell. Hot and cold fluids flow in opposite directions through the inside and outside of the tubes. These types of HEXRs have a very high HTRFR capacity and are used in large-scale applications.

Designing HEXRs is a complex task that requires careful consideration of various factors, including HTRFR yield, PDP, and manufacturing complexity. Parallel flow HEXRs, while popular for their simple design, often present challenges in achieving optimal performance due to limitations in HTRFR compared to counter-flow designs. This research focuses on overcoming these limitations by investigating novel HEXR designs and their impact on key performance parameters.

A comprehensive literature review reveals extensive research on parallel flow HEXRs, particularly SATHECs. Computational Fluid Dynamics (CFD) has emerged as a powerful tool for analyzing and optimizing HEXR designs. Recent research, as evidenced by studies referenced as follows, demonstrates the increasing application of CFD in this field. This study leverages the capabilities of CFD to analyze the performance of novel HEXR designs, aiming to achieve superior yield compared to conventional parallel flow configurations.

Regarding face-to-face research issues, traditional design approaches for parallel flow HEXRs often rely on empirical correlations and established methods. These approaches may not capture intricate flow behavior within complex geometries. Additionally, limitations in manufacturing techniques might restrict the implementation of optimal designs suggested by traditional methods. This research addresses these limitations by employing CFD simulations. Unlike traditional approaches, CFD allows for detailed analysis of flow patterns, pressure distribution, and HTRFR within the HEXR geometry. This enables the exploration of novel designs that may not be feasible with conventional manufacturing techniques and provides valuable insights for future manufacturing advancements.

The Kern and Bell–Delaware methods, which are among the methods used in HEXR design, are also used in shell-side analyses. While the Kern method [1] is preferred over the Bell–Delaware method for preliminary sizing and rough results, the other method can provide much more detailed results in determining the PDP and HTCT [2]. Many numerical and experimental studies have been conducted to improve the thermal performance and flow properties of SATHECs. Generally, the focus is on the effects that worsen the properties of the flow and reduce performance. In the study conducted by Mackley et al., analyses were made on the shell-side HTCT in a cylindrical SATHEC with a BFF [3]. In the study conducted by Chenoweth et al., it was revealed that pressure losses in the exchanger are an

important criterion and that this criterion is important for thermal performance because it is associated with operating costs. Experimental results of isothermal water tests are given for the Reynolds number range from 7000 to 100,000 to evaluate entire and incremental PDPs against division of the HEXR and are related to the flow rate-versus-PDP relationship [4].

In the study by Davies et al., pressure distributions obtained from a comprehensive examination of the shell-side pressure field were used to evaluate the axial dispersion of cross-flow PDP by equipping strategically placed tubes with pressure connections, forming part of the bundle with Reynolds numbers ranging from 270 to 2200 [5]. The study by Gnielinski et al. is based on equations for calculating the PDP with correction factors to calculate the effect of leakage and bypass flows to evaluate the shell-side PDP in SATHECs with sectional baffles. Accordingly, it has been concluded that the separations among experimental measurements and theoretical estimates are within ±35% [6]. Fresh software for the computation, simulation, and optimization of SATHECs was developed by Ajib et al. Thanks to the program, it is possible to predict the effects of deflection gap, deflection plate cut, pipe size, shell size, shell side average HTCT, thermal performance, and thermal yield. Additionally, in the simulations performed to analyze the impact of the pipe pitch on HTRFR, it was concluded that the HTCTs may change when the longitudinal and transverse pipe pitches are changed, and a great settlement was monitored among the literature valuations [7].

In the study conducted by Andrews et al., a three-dimensional numerical model was created and modeled using the k-ϵ model and a Bernoulli type formulation, as well as volumetric porosity and surface permeability, to improve the flow properties in SATHECs. The effectiveness of the baffle cut and baffle interval on PDP was studied. A beneficial settlement was provided among the calculated consequences and the experiments [8]. In the study by Stefanović et al., a numerical study of three-dimensional flow and HTRFR in a SATHEC was carried out. Three different turbulent models were used in the study, which were modeled according to compartment and porous media concepts. Velocity, temperature distributions, and total HTRFR rates were calculated. The impact of dissimilar turbulence patterns on both flow and HTRFR is remarkable. This is due to the inlet effectiveness of eddy viscosity. It is finalized that the Chen–Kim modification of the standard k−ε turbulence model provides the best fit to the experimental datum of the velocity field [9].

The study by Chand et al. includes the effectiveness of the PDP in the inlet and outlet nozzles and the analysis results of the losses in the segments formed by the compartments in the model developed for the shell-side PDP. The model's results for Reynolds numbers between 10^3 and 10^5 match more closely with experimental consequences existing in the literature [10]. According to Reifschneider et al., experiments were carried out to specify the reaction of the HTRFR and PDP on the shell side to the change in distance between the baffles. In the cross-flow region, the per-pipe transfer coefficients corresponding to the smaller BFFSP exceeded those for the larger BFFSP by approximately 5%. The PDP per compartment was reduced as the inter-compartment interval was reduced, but for a constant flow-wise lengthiness, the PDP was observed, resulting in slightly major results for lesser spacings [11]. In the study conducted by Shi et al., four different models of HEXRs were studied. It has been observed that the HTRFR performance of baffles used in models with Reynolds numbers varying between 1000 and 9000 increases [12]. In the study conducted by Tandiroglu, HTRFR effects in turbulent flow were investigated in nine different circular HEXR models using three different baffle orientation angles. Ultimately, they concluded that the proposed correlations were consistent [13]. In the study conducted by Thianpong et al., they carried out an experimental study on entropy generation analysis and thermohydraulic performance by equipping the heat flow tube with a corner-curved BFF. Finally, the results with different Nusselt numbers and angles were transferred to the study [14].

In the study by Lin Li et al., the authors propose a novel method for real-time monitoring of vibrations caused by multiphase-free sink vortex (MFSV) flow in industrial environments. The method combines fluid–structure coupling modeling with vibration

sensing. The key finding is that critical transition states exist during the MFSV evolution, influenced by factors like gas content and flow flux [15]. Scientists are scrutinizing a complex phenomenon known as gas–liquid-coupled vortex flow (GCVF), particularly its behavior at the critical penetration state. To achieve this, they have developed a novel fluid–structure coupling modeling and solution method that leverages the level set and residue theorems. This approach, as demonstrated by their research, offers a deeper understanding of the dynamic evolutionary patterns of GCVF during this critical phase [16]. Another study refines a hybrid analytical–experimental algorithm, empowering engineers to readily predict the effects of disc-doughnut baffles and dimpled tube features on the hydrothermal performance of their baseline SATHEC(s), specifically those with segmental baffles and smooth tubes. The research establishes straightforward analytical–experimental correlations, enabling engineers to perform these calculations with ease and make swift decisions. The key takeaway of this is that utilizing dimpled tubes in conjunction with either segmental or disc-doughnut baffles can significantly enhance the average HTRFR rate of the baseline STHE by an impressive 15.6% and 22.4%, respectively [17]. Vertical SATHEC(s) are the workhorses of industry, valued for their exceptional HTRFR yield, adaptability to various applications, space-saving design, low maintenance requirements, and long lifespan. This research delves into a novel approach to enhance their hydrothermal performance—the implementation of air bubble injection within the shell, utilizing disc and ring baffles with circular holes. This marks a pioneering exploration in this field. Numerical simulations revealed a promising outcome: both these innovative configurations exhibit more uniform velocity and temperature distributions compared to traditional segmental baffles. This uniformity has the potential to significantly improve overall hydrothermal performance [18]. The research goes beyond this initial investigation, aiming to comprehensively analyze the impact of geometrical modifications to the cylindrical shell on the HEXR's performance. This includes factors like PDP, friction factor, exergy, and established performance enhancement criteria (PEC). The findings are expected to demonstrate the positive influence of optimized shell modifications on the system's overall yield and cost-effectiveness [19–22].

When a literature review is made for a newly sized advanced HEXR, it is thought that the size and model of the BFF will guide future HEXR selection and manufacturing.

As a result, we aimed to analyze, for the first time, the PDP, HTCT, and HTRPD values of different types of newly designed HEXRs in these new design geometries, and the new results obtained by taking into account the effects of changes in four different flow rates will guide the manufacture and selection of HEXRs in the future and are introduced to the literature.

2. Materials and Methods

The pathway traced by the fluid in the HEXR model developed in three dimensions, the inlets and outlets of the hot and cold fluids, and the HEXR model, which is analyzed by the computational fluid dynamics method, is given in Figure 1.

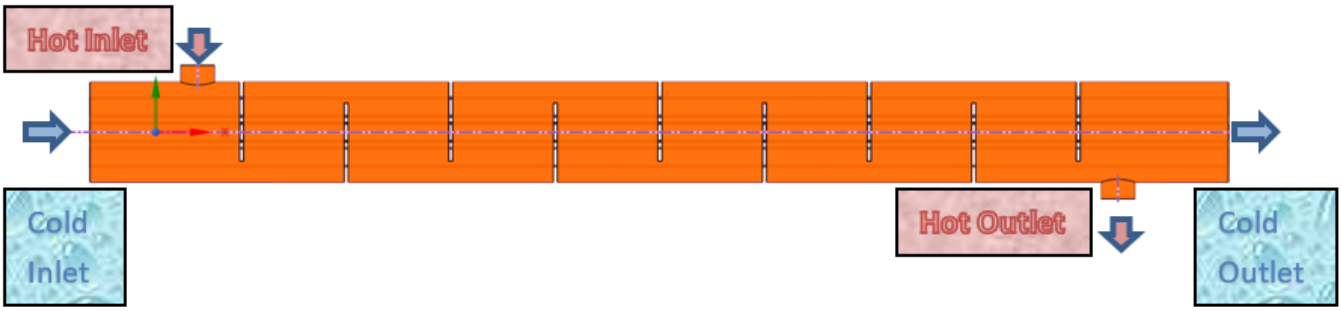

Figure 1. Operating principle.

The modeling strategy is as follows: material and method, physical model, mesh, setup, boarding conditions, analyses, and post-processing operations.

Physical Model

The flowchart for the analysis process is as follows:

Flow Chart

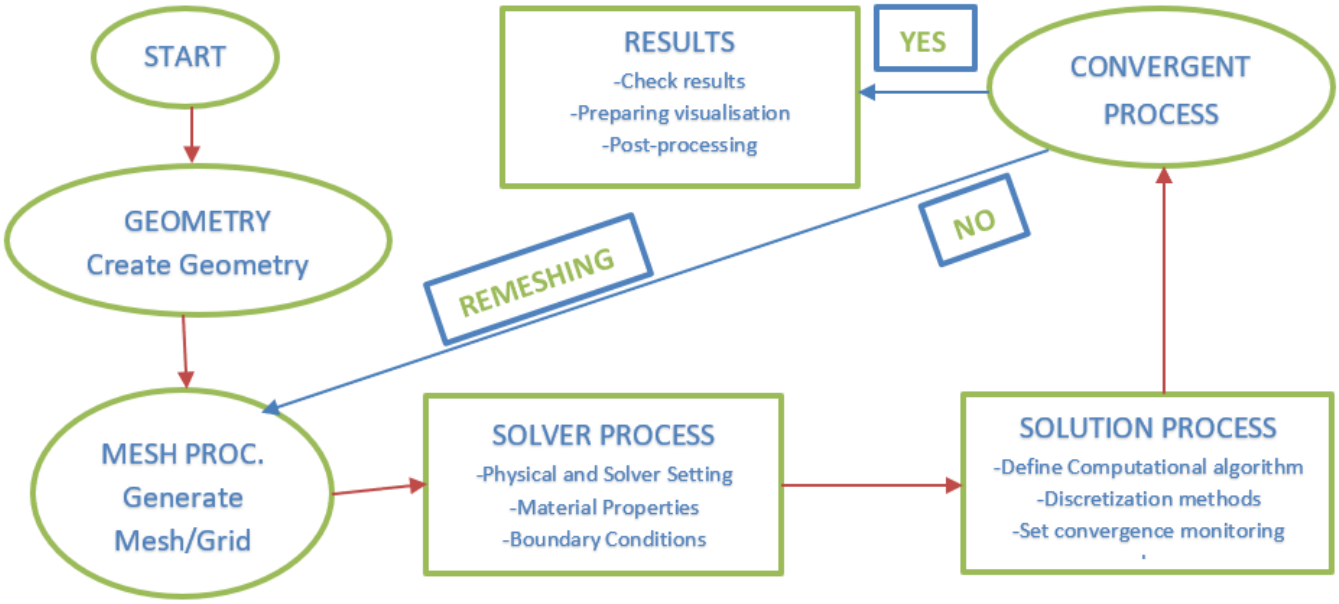

The developed HEXR version, which is 1360 mm linear measurement and 120 mm diameter, consists of a single body and a single pipe passage, together with a summation of five pipes and nine baffles.

Heat exchange and temperature changes occur because of the encounter of hot and cold fluids. Because of this natural physical phenomenon, many research and development products and types of equipment that make our lives easier have emerged. The most important of these is the HEXR. Additionally, with the recent increase in energy consumption and the increased need for energy, the concept of yield has become more prominent. At this point, it is inevitable that the HEXR has added value in terms of yield. Therefore, it is worth dwelling on the issue of PDP in the HEXR and improving HTRFR rates. The effects of these determining factors were examined by changing the gaps between the guiding elements.

Design data for the HEXR are given in Table 1, mesh modeling is given in Figure 2, and baffles designed in different sizes are given in Figure 3. The water thermophysical properties are r = 976 (kg/m^3), c_p = 4191 (J/kg °C), m = 0.00039 (kg/m s), and K = 0.66 (W/m °C).

Table 1. Dimensional chart.

Definition	Size	Definition	Size	Definition	Size
Body		**Pipe**		**Baffle**	
R (mm)	60	D (mm)	24	Number	9
Length (mm)	1360	Sum	5	Thickness (mm)	5
Passes	1	Distance (mm)	6	Gap (mm)	95, 125

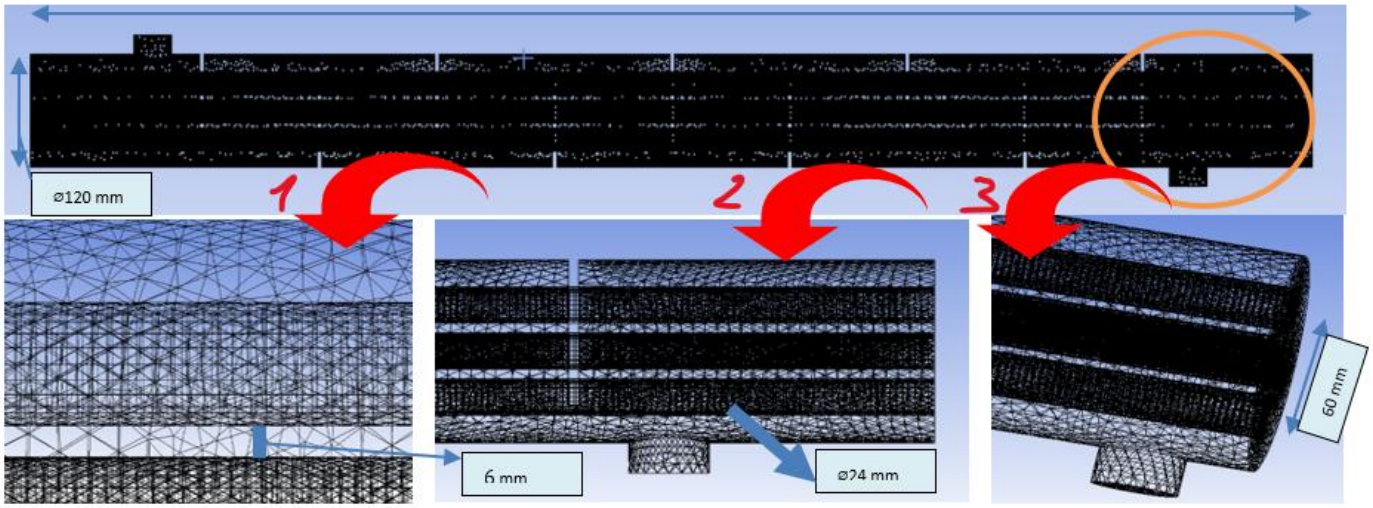

Figure 2. Mesh modeling.

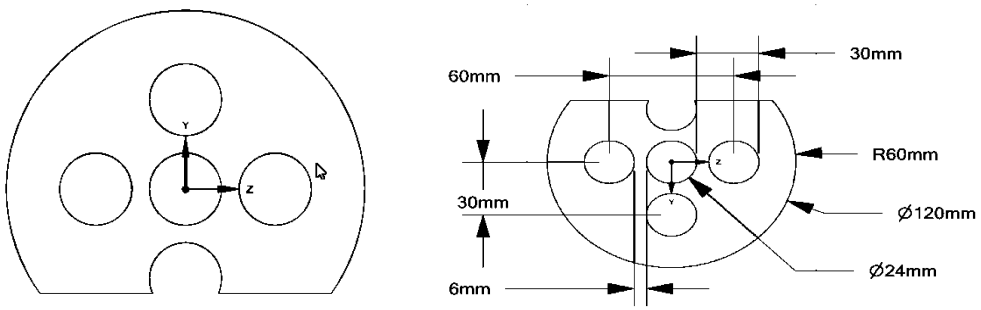

(**a**) (**b**)

Figure 3. (**a**,**b**) BFF modeling.

3. Differential Operations

Turbulence models are related to the type of exchanger and its analysis. RKEM was chosen for the sharper results of the analysis. There are several reasons why RKEM was chosen for the analysis:

Accuracy: RKEM provides a higher level of accuracy than the standard k-ε model. This produces more realistic results, particularly in complex flow fields and swirling flows.

Robustness: RKEM is more robust than the standard k-ε model. It was less prone to convergence problems and performed better at different turbulent Reynolds numbers.

Economy: Although RKEM is more complex than the standard k-ε model, it is still computationally economical. This makes it suitable for large-scale simulation.

Wide range of applications: RKEM can be applied to various turbulent flow problems. These problems include internal and external flows, boundary-layer flows, free flows, and flows with complex geometries.

Some disadvantages of choosing RKEM are as follows:

Complexity: RKEM is more complex than the standard k-ε model and involves a larger number of parameters. This made it difficult to calibrate the model.

Sensitivity: RKEM can be more sensitive to the initial and boundary conditions in certain flow problems.

In conclusion, RKEM offers high accuracy and robustness for the analysis of complex turbulent flows. Its computational economy makes it suitable for several problems. The choice of RKEM depends on the type of problem being analyzed, the desired level of accuracy, and available computational resources.

The other equations are as follows [23].

Continuity equation:

$$\frac{\partial a_i}{\partial l_i} = 0 \tag{1}$$

Momentum equation:

$$A = -\frac{1}{\rho}\frac{\partial p}{\partial l_i} + \frac{\partial}{\partial l_j}\left((\upsilon + \upsilon_t)\left(\frac{\partial a_j}{\partial l_i} + \frac{\partial a_i}{\partial l_j}\right)\right) \tag{2}$$

Energy equation:

$$\frac{\partial a_i\, T}{\partial l_i} = \rho\frac{\partial}{\partial l_i}\left(\left(\frac{\upsilon}{Pr} + \frac{\upsilon t}{Pr}\right)\frac{\partial T}{\partial l_i}\right) \tag{3}$$

Turbulent kinetic energy (k) part:

$$\frac{\partial a_i\, z}{\partial l_i} = \frac{\partial}{\partial l_i}\left[\left(\upsilon + \frac{\upsilon t}{\sigma_z}\right)\frac{\partial k}{\partial x_i}\right] + \Gamma - \varepsilon \tag{4}$$

Turbulent energy dissipation (ε) part:

$$\frac{\partial a_i\, \varepsilon}{\partial l_i} = \frac{\partial}{\partial l_i}\left[\left(\upsilon + \frac{\upsilon t}{\sigma_\varepsilon}\right)\frac{\partial \varepsilon}{\partial l_i}\right] + c_1\Gamma\varepsilon - c_2\frac{\varepsilon^2}{z + \sqrt{\upsilon\varepsilon}} \tag{5}$$

The production of turbulent kinetic energy z with "Γ" is shown in Equations (4) and (5) [24].

$$\Gamma = -\overline{a_i\, a_j}\frac{\partial a_i}{\partial l_i} = \upsilon_t\left(\left(\frac{\partial a_i}{\partial l_j} + \frac{\partial a_j}{\partial l_i}\right)\frac{\partial a_i}{\partial l_i}\right) \tag{6}$$

$$\upsilon_t = c_\mu\frac{z^2}{\varepsilon} \tag{7}$$

3.1. Energy Balance in a SATHEC

The basic principle of energy balance states that, within a steady-state system, the total energy entering the system must equal the total energy leaving the system. In a SATHEC, we can apply this principle to analyze the HTRFR between the hot and cold fluids. Here is a breakdown of the energy balance for a SHE:

3.2. Incoming Energy

Hot fluid: The hot fluid entering the exchanger carries thermal energy due to its MFRT (ṁ_h) and specific heat capacity (Cp_h) at its inlet temperature (T_hi). This can be expressed as follows:

$$Q\_h\_in = \dot{m}\_h \times Cp\_h \times (T\_hi) \tag{8}$$

3.3. Outgoing Energy

Hot fluid: The hot fluid exits the exchanger at a lower temperature (T_ho) after transferring heat to the cold fluid. The thermal energy carried out by the hot fluid is as follows:

$$Q\_h\_out = \dot{m}\_h \times Cp\_h \times (T\_ho) \tag{9}$$

Cold fluid: The cold fluid enters the exchanger at a lower temperature (T_ci) and absorbs heat, increasing its temperature to T_co. The thermal energy gained from cold fluids is as follows:

$$Q\_c = \dot{m}\_c \times Cp\_c \times (T\_co - T\_ci) \tag{10}$$

3.4. Heat Transfer

The heat transferred (Q) from the hot fluid to the cold fluid is what we are primarily interested in. In a steady-state system, this HTRFR must equal the difference between the incoming and outgoing thermal energies of the hot fluid.

$$Q = Q\_h\_in - Q\_h\_out \quad (11)$$

3.5. Applying Energy Balance

By setting the heat transferred (Q) equal to the thermal energy gained by the cold fluid (Q_c), we obtain the energy balance equation for the SATHEC:

$$ṁ\_h \times Cp\_h \times (T\_hi - T\_ho) = ṁ\_c \times Cp\_c \times (T\_co - T\_ci) \quad (12)$$

This equation allows us to calculate various parameters in the HEXR, such as the outlet temperatures of the fluids or the required flow rates for a desired HTRFR rate (Q).

3.6. Additional Considerations

In some cases, there might be heat losses to the environment (Q_loss). This term can be added to the energy balance equation to account for these losses.

The effectiveness of a HEXR depends on its ability to maximize HTRFR between the fluids. This is often analyzed using parameters like effectiveness (ε), which relate the actual HTRFR to the maximum theoretical HTRFR achievable under specific conditions.

By understanding and applying the energy balance principle, engineers can design and analyze SATHEC(s) for various industrial applications.

3.7. Boundary Conditions

The importance of limiting values in the design of HEXRs can be striking. The effect of limiting values on the analysis can be observed in the results using the computational fluid dynamics method. Analyses were carried out in an environment where gravity effects and leaks were neglected in the steady regime, assuming that HTRFR did not occur outside the body. Analyses were carried out using standard wall functions and applying a non-slip boundary condition to the surfaces, where the inlet temperature was 62 °C and the surface temperature of the pipe was 17 °C. As a result, the analysis results of fluid behavior, PDP, and HTRFR rate in cases where BFFSPs were 95 mm and 125 mm were examined.

3.8. Mesh Independence Test

Pressure and temperature effects in HEXRs are important in terms of the size of the yield obtained. Mesh independence testing also forms part of this, providing a better understanding of these effects. This test constitutes an important step in ensuring the accuracy of computational fluid dynamics analyses. In this study, five different network systems were created with the number of elements: 965,417, 612,208, 246,834, 108,673, and 96,297. The exit temperature variation between the last two mesh grids was found to be less than 1%. Based on this, it was concluded that the mesh grid with 108,673 elements was sufficient for the flow analysis process, and the research was conducted accordingly. Figure 4a presents the analysis results.

The mesh independence test is shown with point details in Figure 4a. The skewness value belonging to the mesh quality is also shown in Figure 4b.

In Figure 4b, the skewness value of the mesh quality was checked. Accordingly, the closer the skewness value is to zero, the better the mesh quality; with a higher quality, the analysis can be continued at a level that means the operations can be continued. As can be seen in Figure 4b, the skewness value is concentrated between 0.10–0.26. The mesh quality is good, and it was concluded that the analysis can be continued.

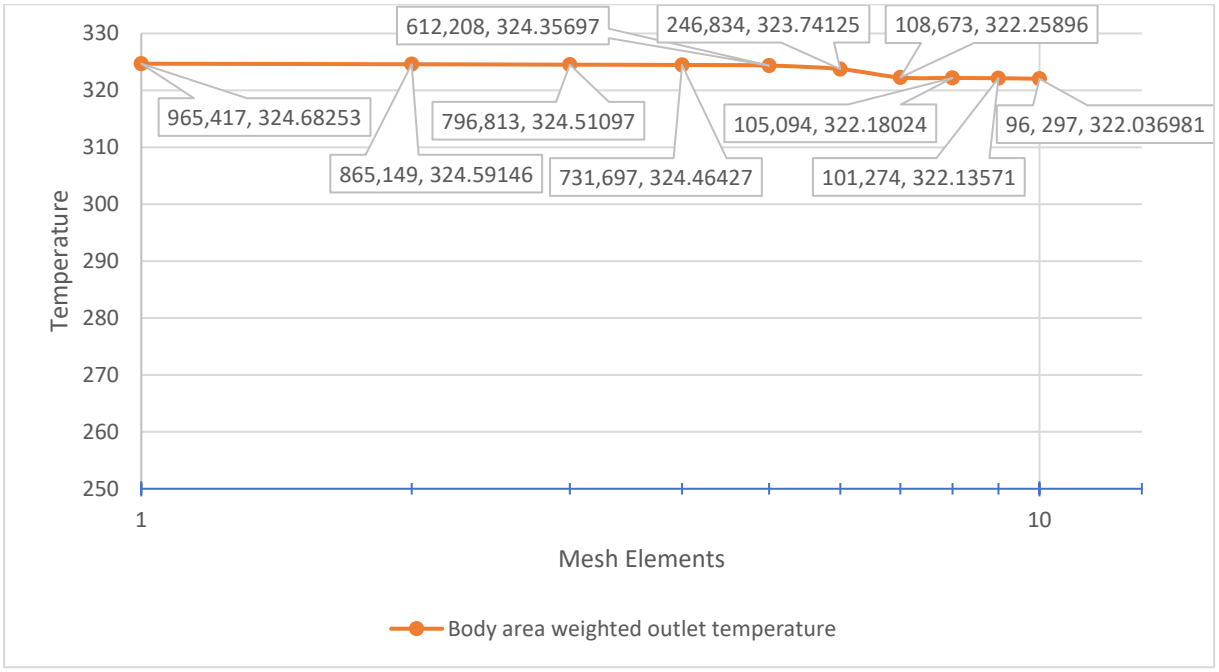

(**a**)

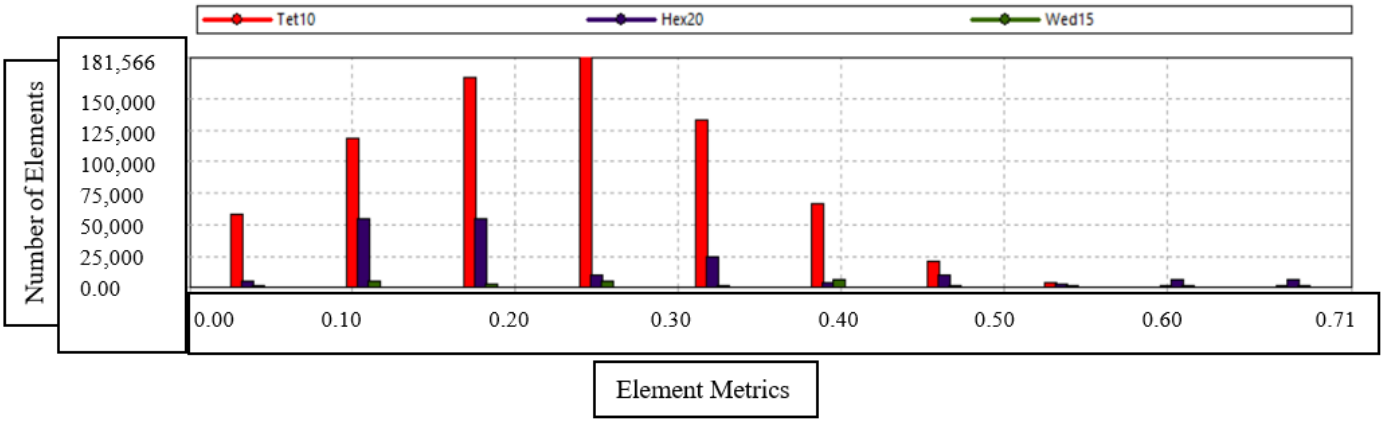

(**b**)

Figure 4. (**a**) Mesh independence test, (**b**) mesh quality of skewness.

3.9. Data Reduction

To operate the knowledge gathered from the analyses, the analyst used an intense equation to work out both the shell-side HTC (ks) and the HTRFR rate. The equation is as follows:

$$k_h = \frac{[Body\ Heat\ Transfer = Q_s = \dot{m}\ h \cdot cp, h \cdot (Kh, i - Kh, o)]}{\text{Ah}} \tag{13}$$

$$Ah = N \cdot \pi \cdot d0 \cdot L \cdot \left(\frac{[Kh, i - Kw] \ - [Kh, o - Kw]}{ln \frac{[Kh, i - Kw]}{[Kh, o - Kw]}} \right) \tag{14}$$

4. Results and Discussion

HEXRs play a crucial role in various industrial processes, and their yield directly translates to significant economic and operational benefits. This study delves into the impact of BFFSP on a HEXR's output, specifically focusing on its influence on HTCT and PDP.

The investigation hinges on the understanding that even minor changes in the HEXR design can significantly alter fluid behavior within the unit. This research meticulously analyzes the contrasting fluid behavior observed with two distinct BFFSP configurations: 95 mm and 125 mm.

Furthermore, the study goes beyond a basic comparison by incorporating the influence of MFRTs on the HEXR's output. Four different MFRs (0.1 kg/h, 0.3 kg/h, 0.5 kg/h, and 0.7 kg/h) are analyzed to comprehensively understand how they interact with the BFFSP to affect both PDP and HTCT.

The results reveal fascinating trends. It was observed that for all the investigated MFRs (0.1 kg/h, 0.3 kg/h, 0.5 kg/h, and 0.7 kg/h), the outlet temperature consistently remained higher in the model with a 125 mm BFFSP compared to the one with a 95 mm spacing. This suggests that wider spacing might be hindering efficient HTRFR, leading to a higher outlet temperature on the heated fluid side.

However, the story takes a fascinating turn when considering the PDP. The study found the opposite effect for PDP. In all MFR scenarios (0.1 kg/h, 0.3 kg/h, 0.5 kg/h, and 0.7 kg/h), the model with a 95 mm BFFSP exhibited a lower PDP compared to the model with a 125 mm gap. This indicates that the closer BFF arrangement promotes a more streamlined flow, resulting in a lower PDP across the HEXR.

These findings highlight the intricate interplay between BFFSP, MFR, and the overall output of a HEXR. While wider spacing might lead to slightly higher outlet temperatures, it potentially comes at the cost of increased PDPs. Conversely, closer BFF arrangements, despite offering a lower PDP, might compromise HTRFR yield.

This detailed exploration underscores the importance of optimizing BFFSP in HEXR design. By carefully considering the specific application and desired balance between thermal performance and PDP, engineers can tailor the HEXR configuration to maximize its effectiveness and contribute to both user savings and overall added value.

In Figure 5, the effects of fluid behavior on temperature when the MFRT is 0.1 kg/h are simulated in the developed geometry model with 95 mm BFF spacing. Here, the cold water entering at 290 K meets the hot water entering at 335 K within the 95 mm baffle gap. In addition, progress has been made in thermal conductivity by making the body material from aluminum. Thermal conductivity was analyzed as 202.4 W/mK and specific heat as 871 J/kgK.

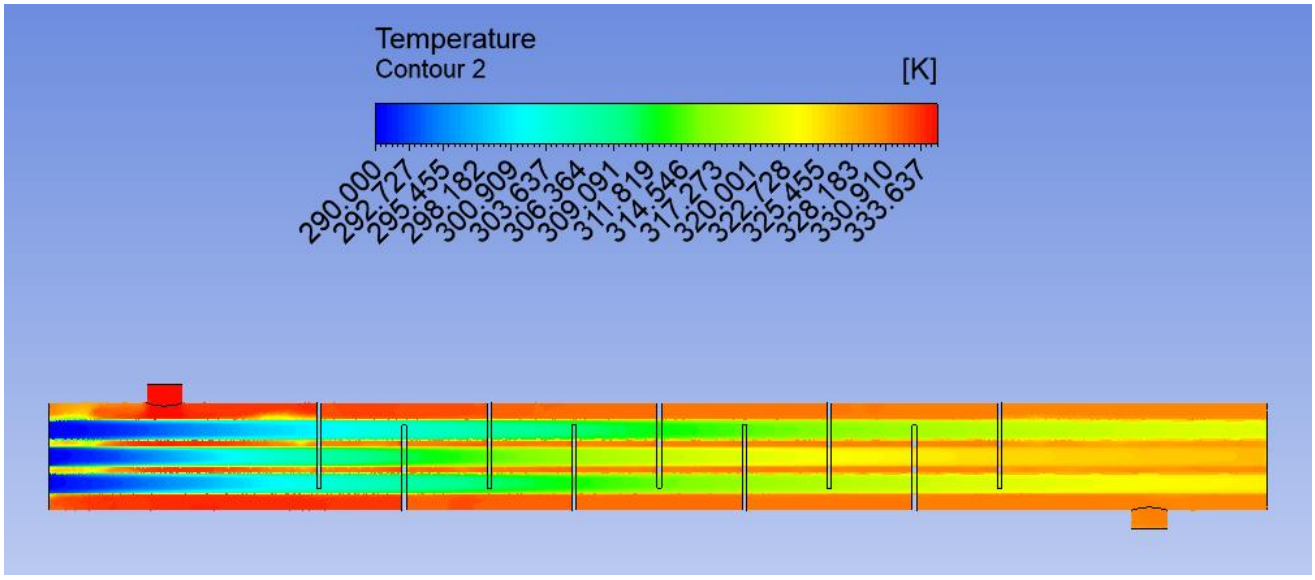

Figure 5. Temperature apportionment of upgraded geometry at multifarious baffle spreads, gap = 95 mm, flowrate = 0.1 kg/h.

In Figure 6, the effectiveness of fluid behavior on pressure when the MFRT is 0.1 kg/h is simulated in the developed geometry model with 95 mm BFF spacing. Here, the cold water entering at 290 K meets the hot water entering at 335 K within the 95 mm baffle gap. In addition, progress has been made in thermal conductivity by making the body material from aluminum. Thermal conductivity was analyzed as 202.4 W/mK and specific heat as 871 J/kgK.

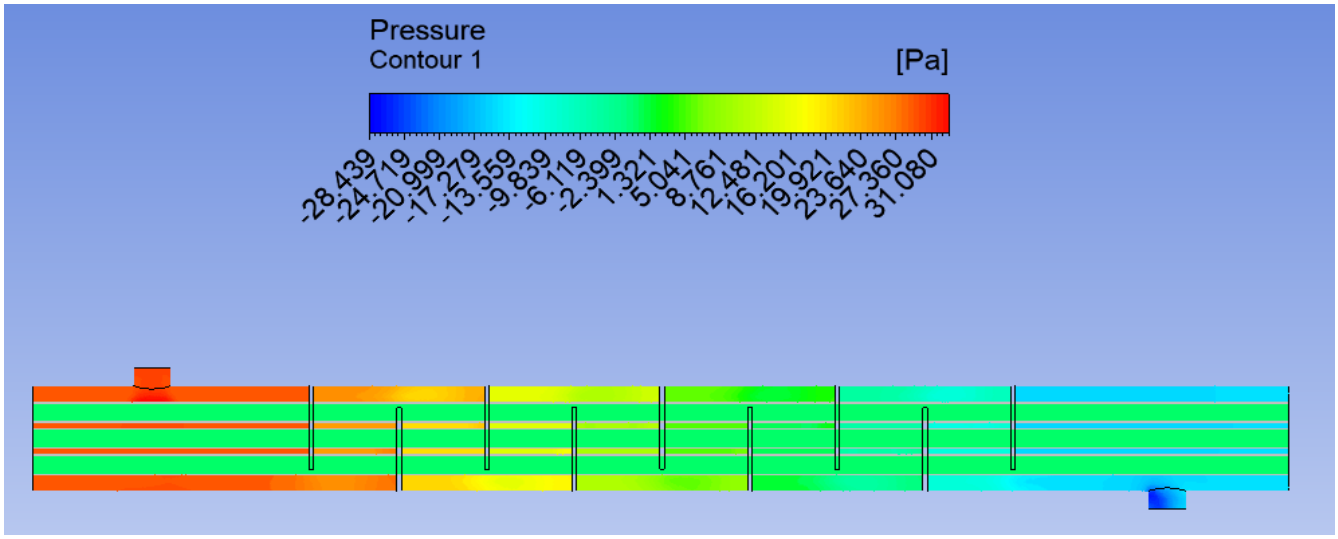

Figure 6. Pressure apportionment of upgraded geometry at multifarious baffle spreads, gap = 95 mm, flowrate = 0.1 kg/h.

In Figure 7, the effects of fluid behavior on pressure when the MFRT is 0.1 kg/h are simulated in the developed geometry model with 125 mm BFF spacing. Here, the cold water entering at 290 K meets the hot water entering at 335 K within the 125 mm baffle gap.

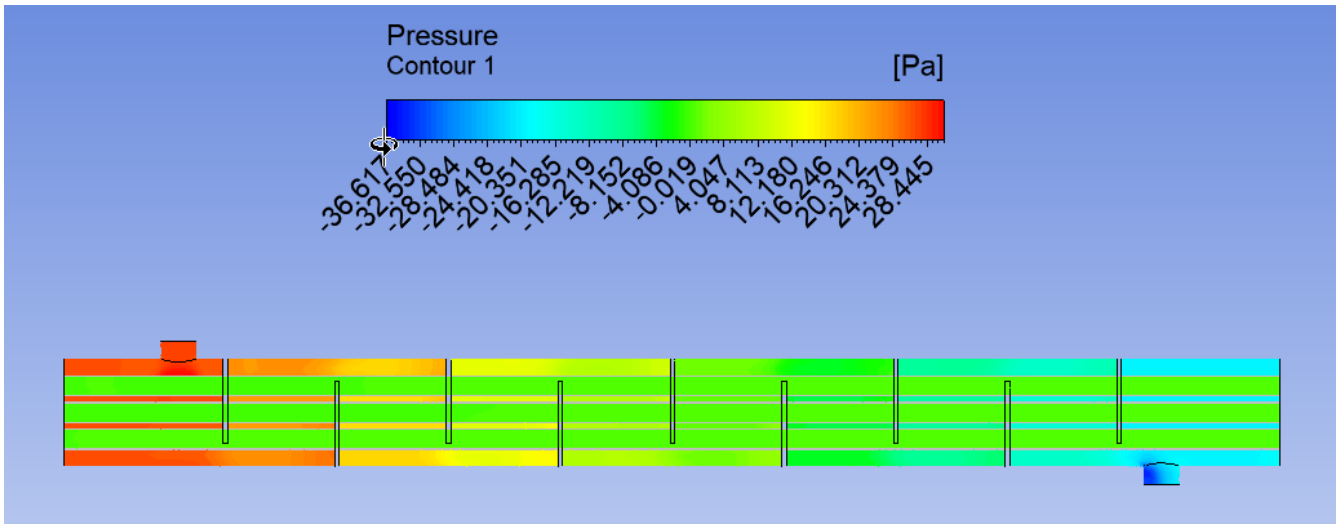

Figure 7. Pressure apportionment of upgraded geometry at multifarious baffle spreads, gap = 125 mm, flowrate = 0.1 kg/h.

In Figure 8, the effects of fluid behavior on temperature when the MFRT is 0.1 kg/h are simulated in the developed geometry model with 125 mm BFF spacing. Here, the cold water entering at 290 K meets the hot water entering at 335 K within the 125 mm baffle gap.

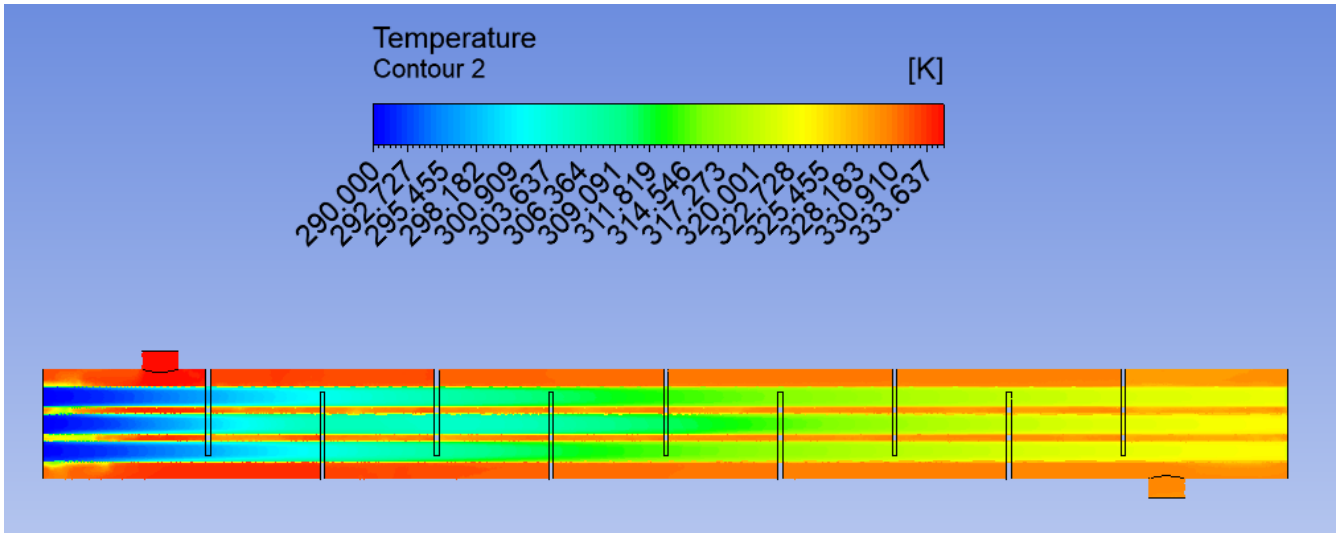

Figure 8. Temperature apportionment of upgraded geometry at multifarious baffle spreads, gap = 125 mm, flowrate = 0.1 kg/h.

In Figure 9, the effects of fluid behavior on pressure when the MFRT is 0.3 kg/h are simulated in the developed geometry model with 95 mm BFF spacing. Here, the cold water entering at 290 K meets the hot water entering at 335 K within the 125 mm baffle gap.

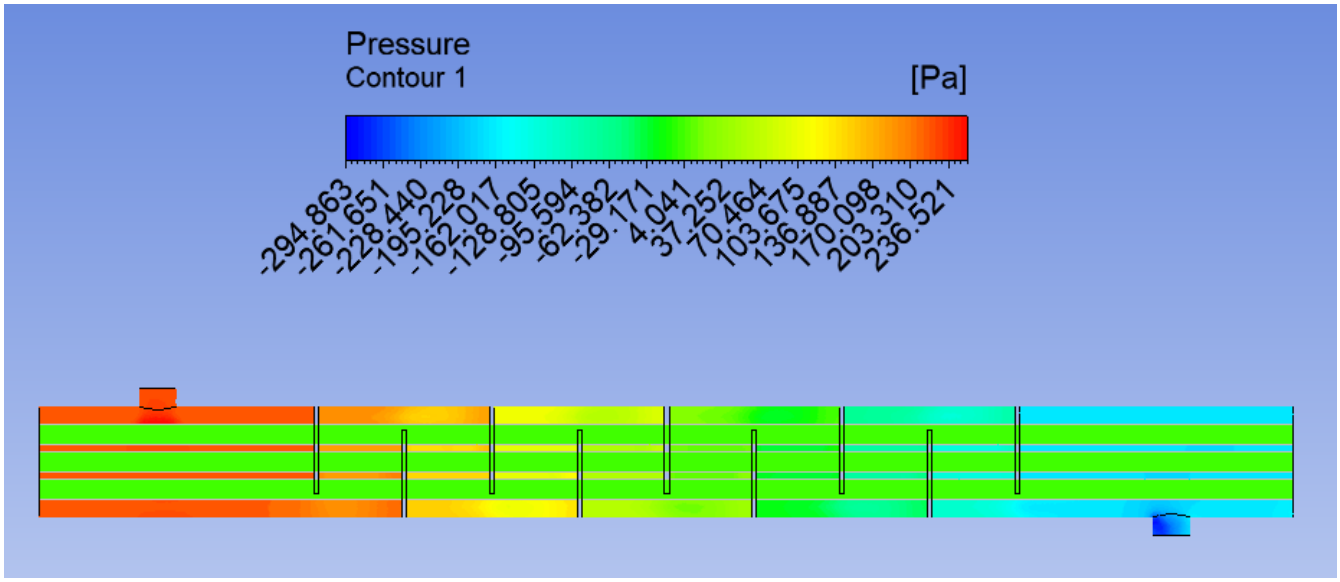

Figure 9. Pressure apportionment of upgraded geometry at multifarious baffle spreads, gap = 95 mm, flowrate = 0.3 kg/h.

In Figure 10, the effects of fluid behavior on temperature when the MFRT is 0.3 kg/h are simulated in the developed geometry model with 95 mm BFF spacing. Here, the cold water entering at 290 K meets the hot water entering at 335 K within the 125 mm baffle gap.

In Figure 11, the effects of fluid behavior on pressure when the MFRT is 0.3 kg/h are simulated in the developed geometry model with a BFF spacing of 125 mm. Here, the cold water entering at 290 K meets the hot water entering at 335 K within the 125 mm baffle gap.

In Figure 12, the effects of fluid behavior on temperature when the MFRT is 0.3 kg/h are simulated in the developed geometry model with 125 mm BFF spacing. Here, the cold water entering at 290 K meets the hot water entering at 335 K within the 125 mm baffle gap.

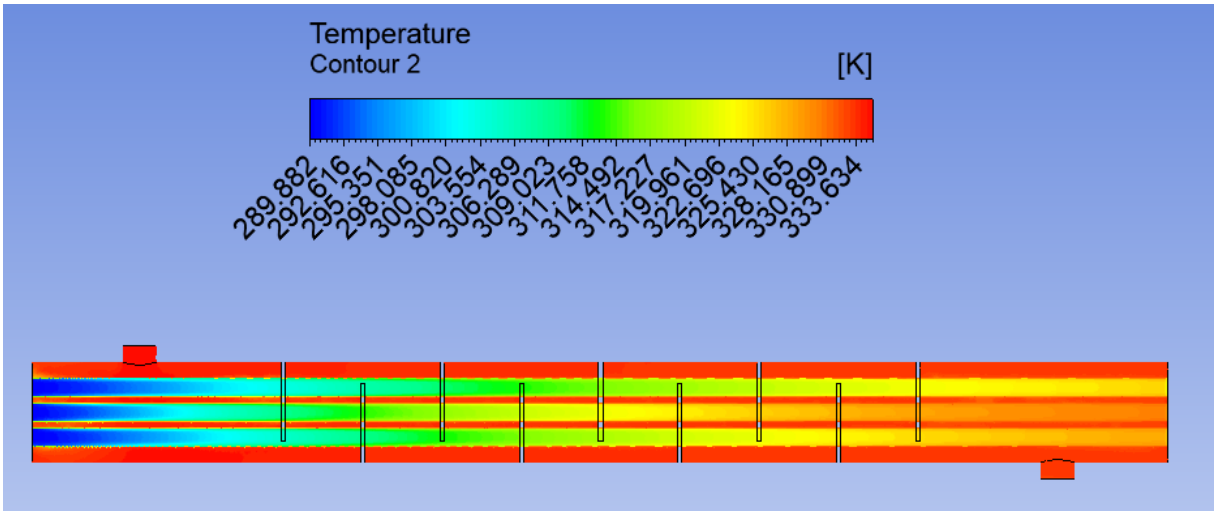

Figure 10. Temperature apportionment of upgraded geometry at multifarious baffle spreads, gap = 95 mm, flowrate = 0.3 kg/h.

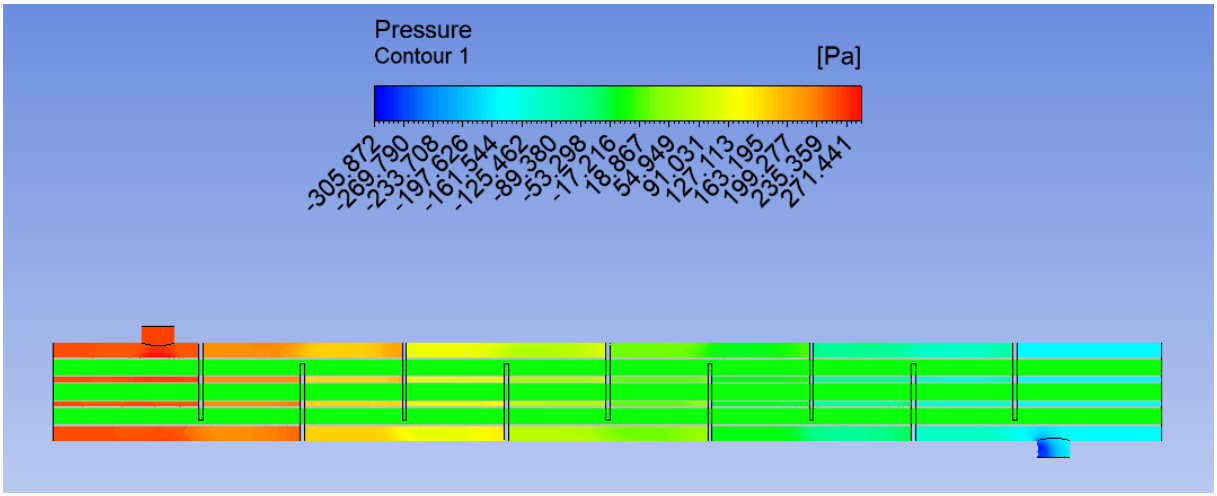

Figure 11. Pressure apportionment of upgraded geometry at multifarious baffle spreads, gap = 125 mm, flowrate = 0.3 kg/h.

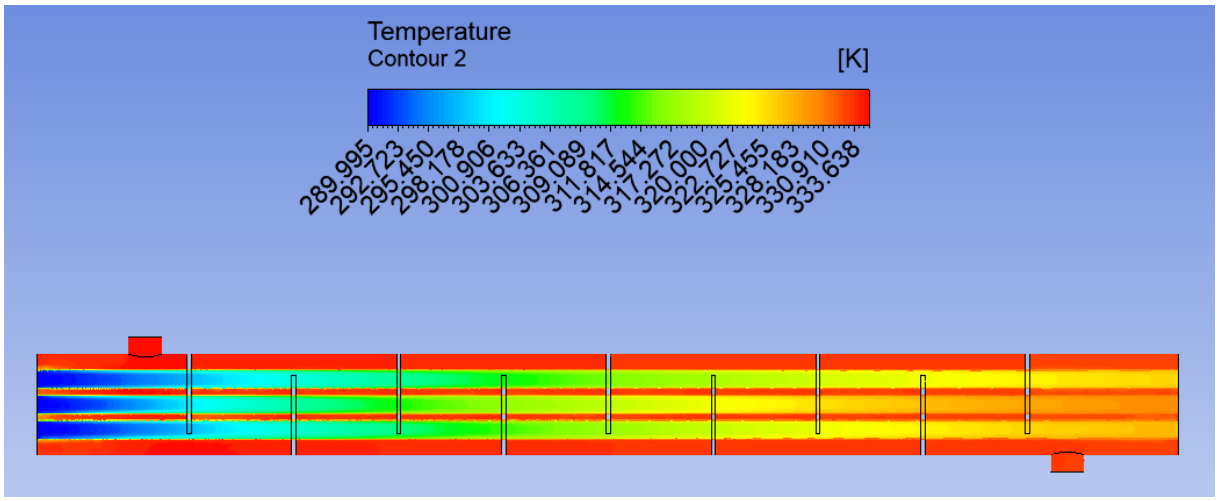

Figure 12. Temperature apportionment of upgraded geometry at multifarious baffle spreads, gap = 125 mm, flowrate = 0.3 kg/h.

In Figure 13, the effects of fluid behavior on temperature when the MFRT is 0.5 kg/h are simulated in the developed geometry model with 95 mm BFF spacing. Here, the cold water entering at 290 K meets the hot water entering at 335 K within the 125 mm baffle gap.

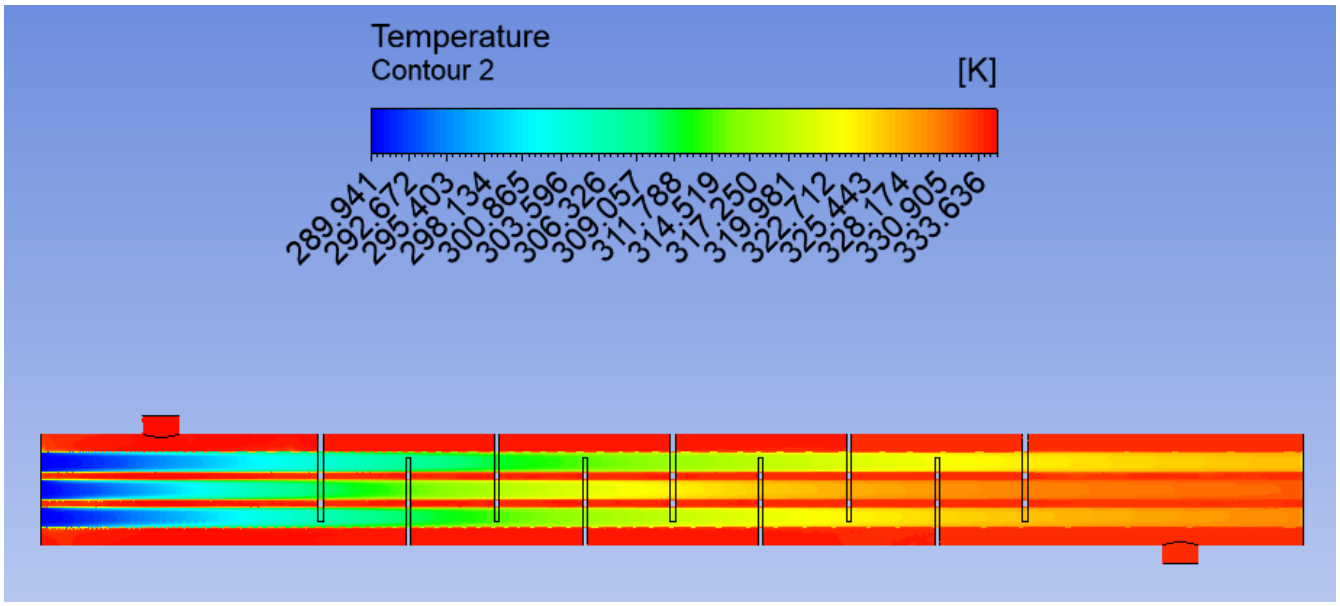

Figure 13. Temperature apportionment of upgraded geometry at multifarious baffle spreads, gap = 95 mm, flowrate = 0.5 kg/h.

In Figure 14, the effects of fluid behavior on pressure when the MFRT is 0.5 kg/h are simulated in the developed geometry model with 95 mm BFF spacing. Here, the cold water entering at 290 K meets the hot water entering at 335 K within the 125 mm baffle gap.

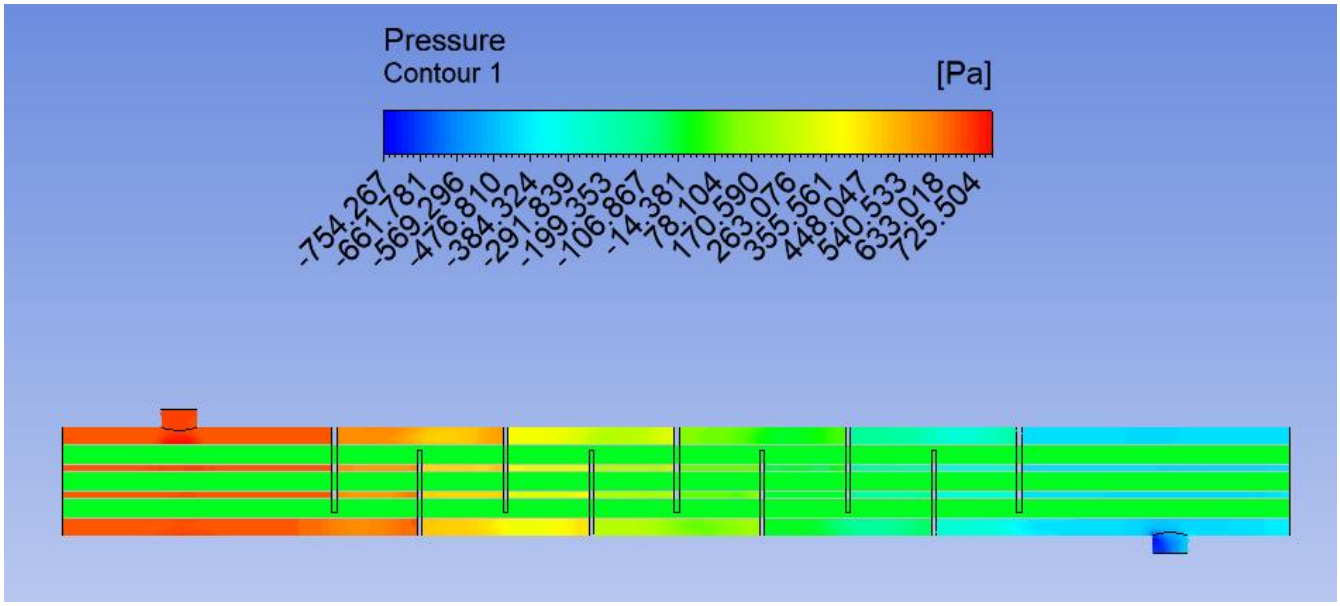

Figure 14. Pressure apportionment of upgraded geometry at multifarious baffle spreads, gap = 95 mm, flowrate = 0.5 kg/h.

In Figure 15, the effects of fluid behavior on pressure when the MFRT is 0.5 kg/h are simulated in the developed geometry model with 125 mm BFF spacing. Here, the cold water entering at 290 K meets the hot water entering at 335 K within the 125 mm baffle gap.

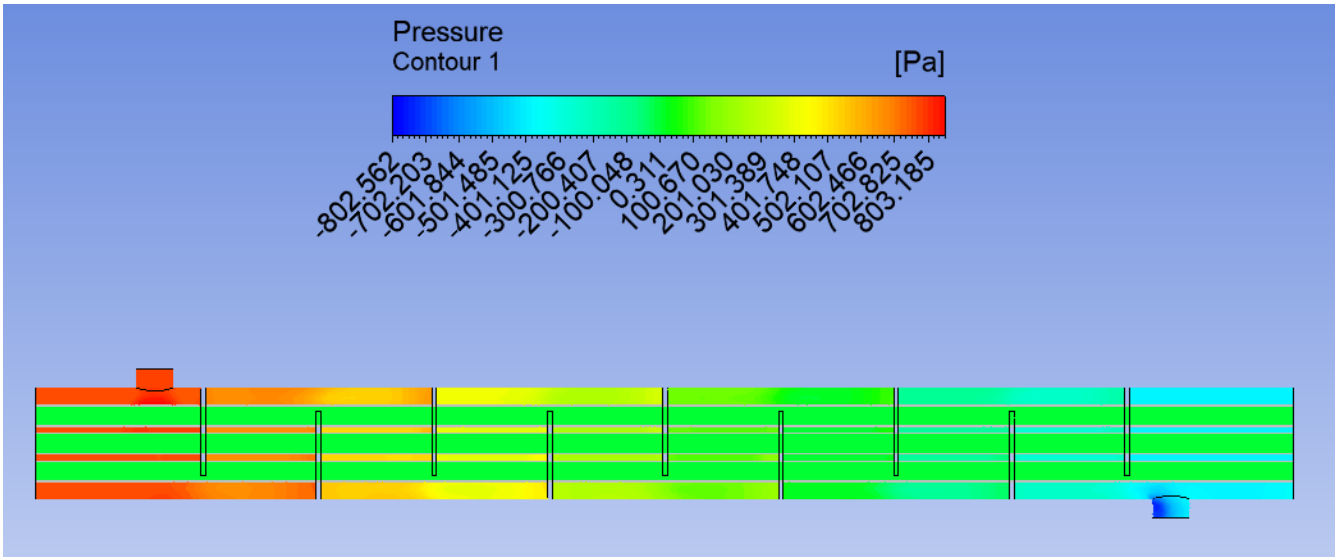

Figure 15. Pressure apportionment of upgraded geometry at multifarious baffle spreads, gap = 125 mm, flowrate = 0.5 kg/h.

In Figure 16, the effects of fluid behavior on temperature when the MFRT is 0.5 kg/h are simulated in the developed geometry model with 125 mm BFF spacing. Here, the cold water entering at 290 K meets the hot water entering at 335 K within the 125 mm baffle gap.

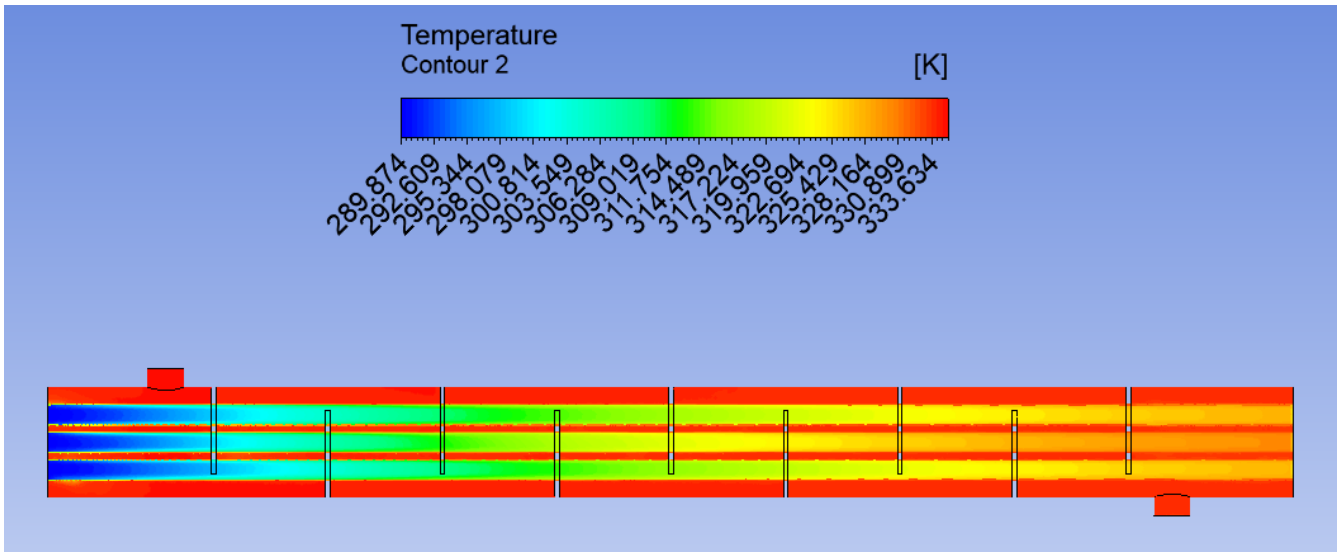

Figure 16. Temperature apportionment of upgraded geometry at multifarious baffle spreads, gap = 125 mm, flowrate = 0.5 kg/h.

In Figure 17, the effects of fluid behavior on temperature when the MFRT is 0.7 kg/h are simulated in the developed geometry model with 95 mm BFF spacing. Here, the cold water entering at 290 K meets the hot water entering at 335 K within the 125 mm baffle gap.

In Figure 18, the effects of fluid behavior on pressure when the MFRT is 0.7 kg/h are simulated in the developed geometry model with 95 mm BFF spacing. Here, the cold water entering at 290 K meets the hot water entering at 335 K within the 125 mm baffle gap.

In Figure 19, the effects of fluid behavior on pressure when the MFRT is 0.7 kg/h are simulated in the developed geometry model with 125 mm BFF spacing. Here, the cold water entering at 290 K meets the hot water entering at 335 K within the 125 mm baffle gap.

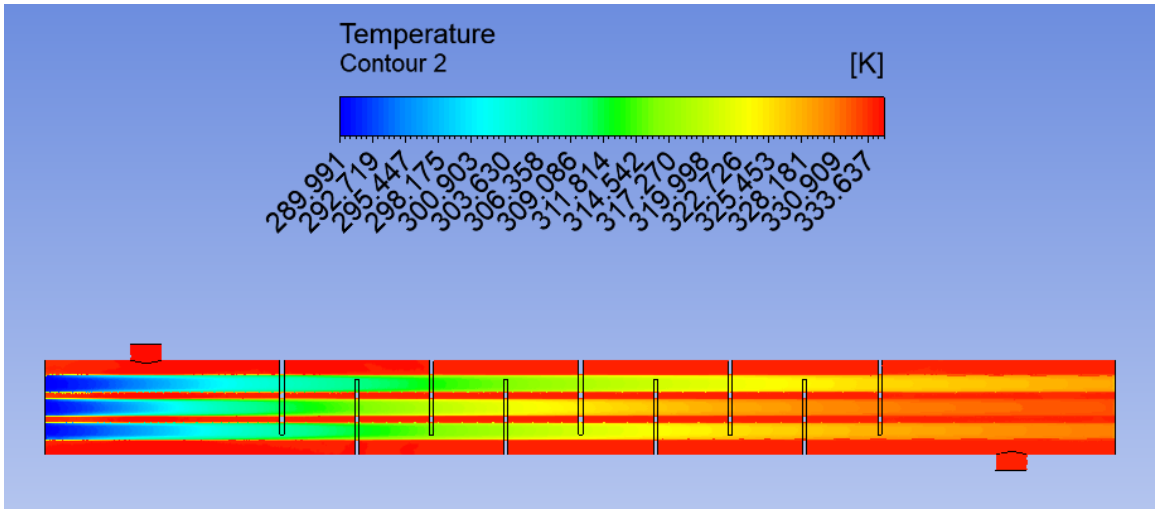

Figure 17. Temperature apportionment of upgraded geometry at multifarious baffle spreads, gap = 95 mm, flowrate = 0.7 kg/h.

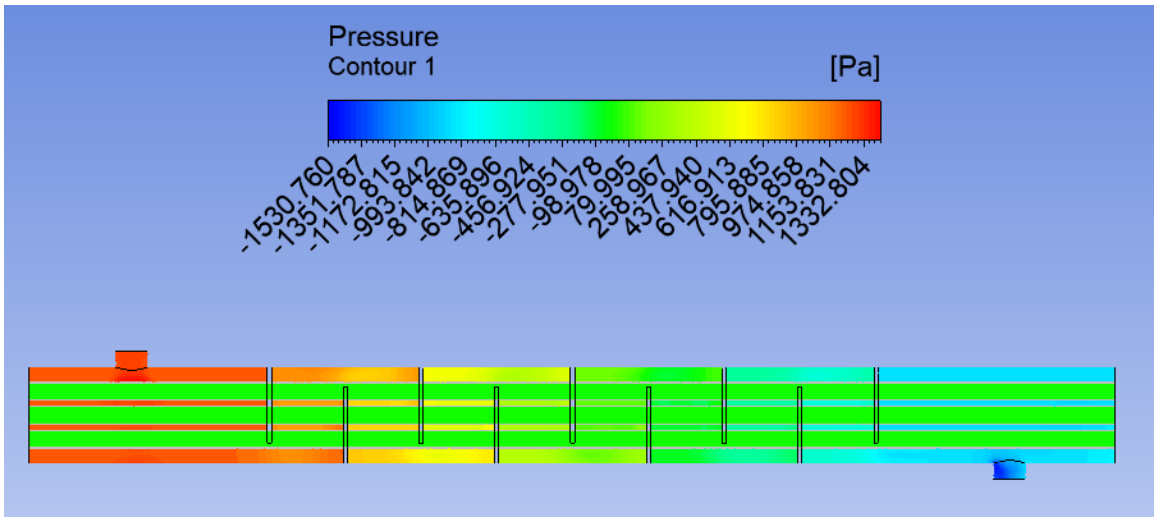

Figure 18. Pressure apportionment of upgraded geometry at multifarious baffle spreads, gap = 95 mm, flowrate = 0.7 kg/h.

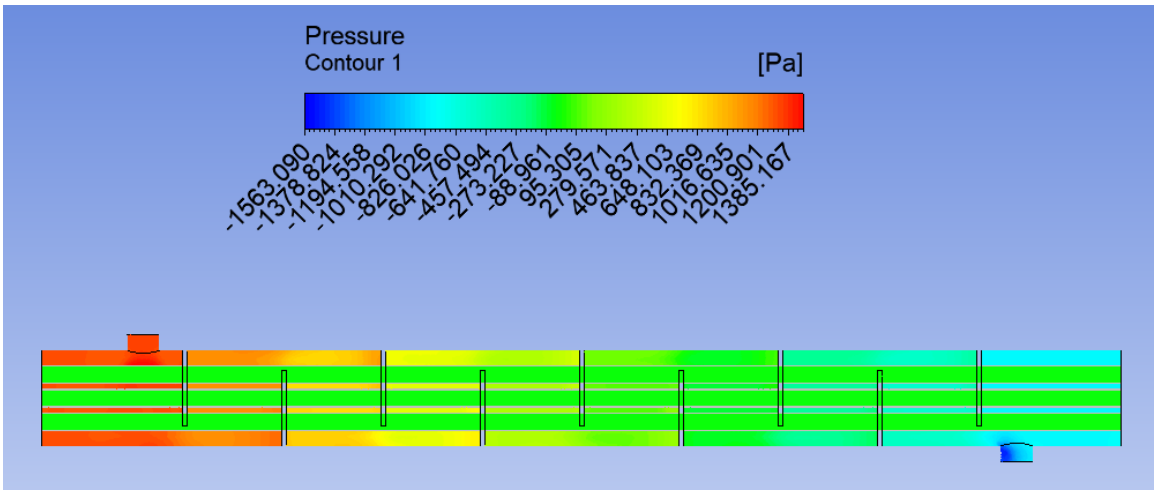

Figure 19. Pressure apportionment of upgraded geometry at multifarious baffle spreads, gap = 125 mm, flowrate = 0.7 kg/h.

In Figure 20, the effects of fluid behavior on temperature when the MFRT is 0.7 kg/h are simulated in the developed geometry model with 125 mm BFF spacing. Here, the cold water entering at 290 K meets the hot water entering at 335 K within the 125 mm baffle gap.

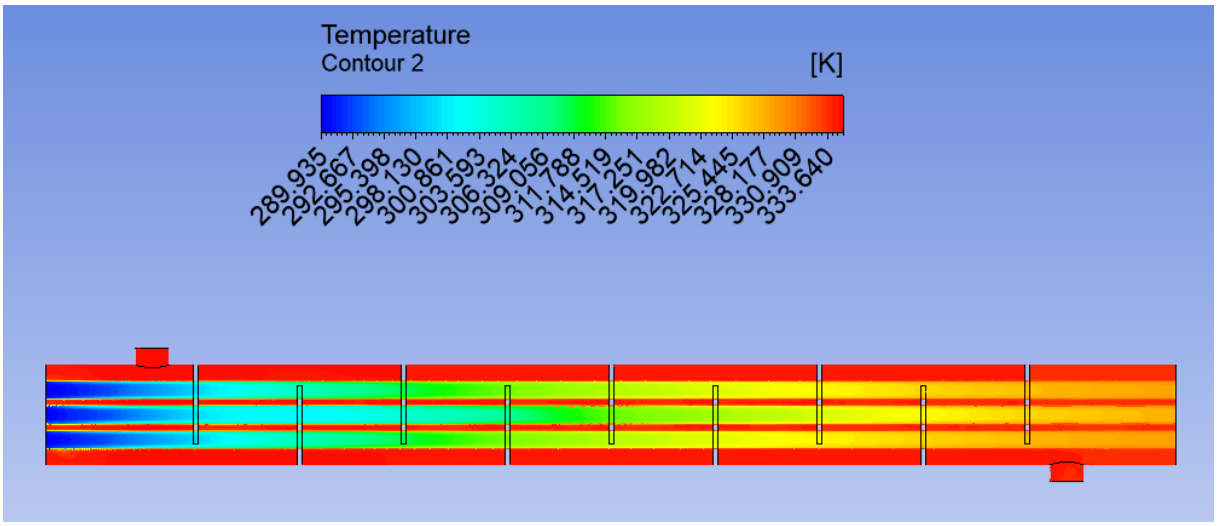

Figure 20. Temperature apportionment of upgraded geometry at multifarious baffle spreads, gap = 125 mm, flowrate = 0.7 kg/h.

In Figure 21, the effects of fluid behavior on velocity when the MFRT is 0.7 kg/h are simulated in the developed geometry model with 95 mm BFFSP. Here, the cold water entering at 290 K meets the hot water entering at 335 K within the 95 mm baffle gap. Figure 21 shows how BFFs promote the turbulent flow of the fluid inside the tubes. The highest velocity is observed near the BFFs. The fluid velocity decreases toward the center of the tubes. The number and spacing of BFFs have a significant effect on fluid velocity and HTRFR.

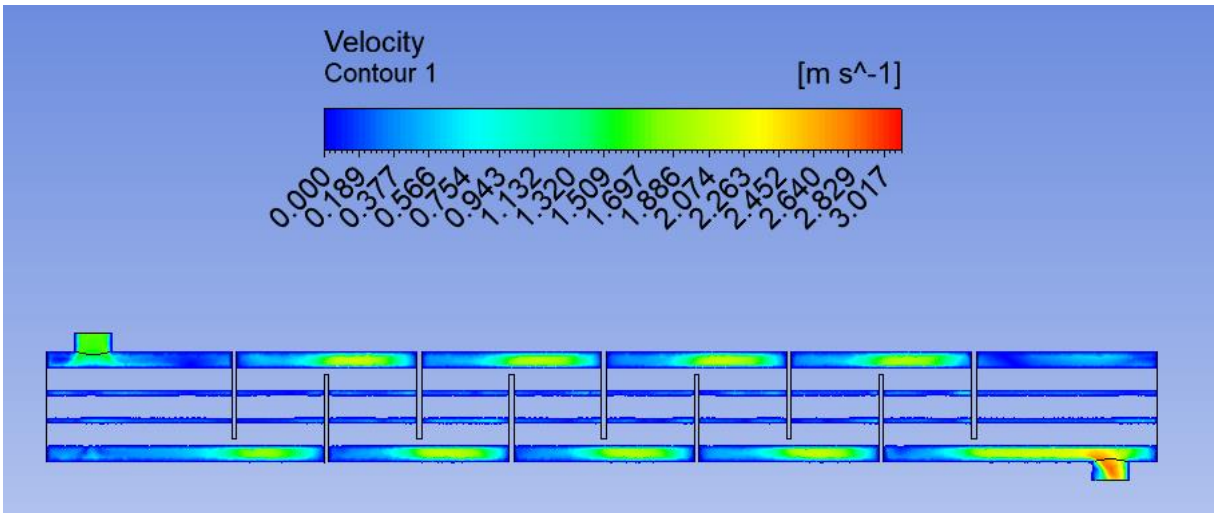

Figure 21. Velocity apportionment of upgraded geometry at multifarious baffle spreads, gap = 95 mm, flowrate = 0.7 kg/h.

Figure 22 shows the relationship between HTCT and MFRT. The effects of fluid behavior varying between two different baffle intervals of 95 mm and 125 mm can be defined by the changes in MFRT on the HTCT. Accordingly, in cases where the MFRT is 0.1 kg/h, 0.3 kg/h, 0.5 kg/h, and 0.7 kg/h, for all compartment intervals where the

designed model is 95 mm and 125 mm, it could be observed that the HTCT increased accordingly. According to the conclusion drawn from Figure 22, in all cases where the MFRT of the model in geometry with 125 mm BFFSP is 0.1 kg/h, 0.3 kg/h, 0.5 kg/h, and 0.7 kg/h, it can be concluded that it has a smaller HTCT than the other model with 95 mm BFFSP.

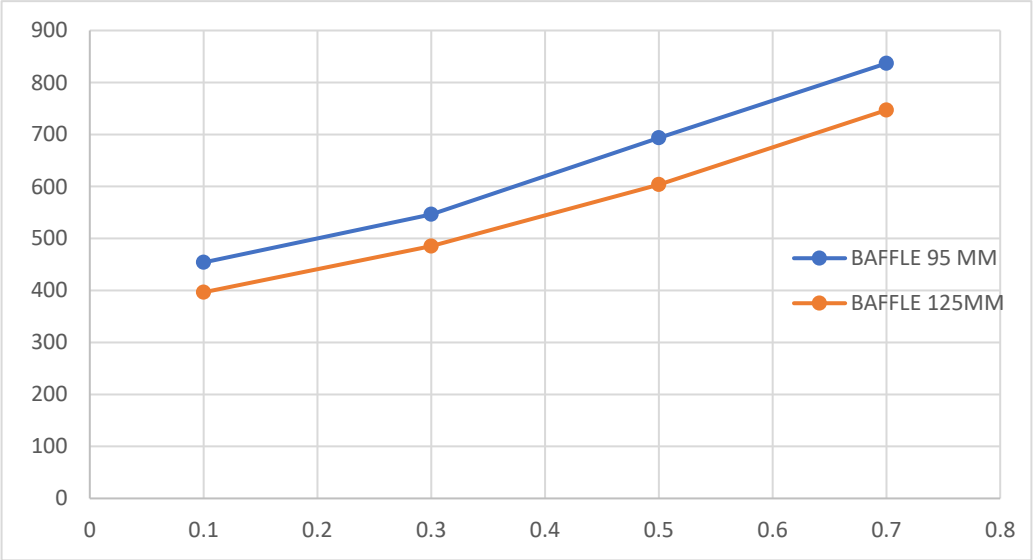

Figure 22. HTC for MFR at two baffle distances: 95 mm and 125 mm.

Figure 23 shows the relationship between MFRT and PDP. The effects of fluid behavior varying between two different baffle intervals of 95 mm and 125 mm can be defined by changes in MFRT on PDP. Accordingly, it can be observed that the PDP increases accordingly when the MFRT increases to 0.1 kg/h, 0.3 kg/h, 0.5 kg/h, and 0.7 kg/h for all compartment intervals where the designed model is 95 mm and 125 mm. According to the conclusion drawn from Figure 23, in all cases where the MFRT of the model in geometry with 125 mm BFFSP is 0.1 kg/h, 0.3 kg/h, 0.5 kg/h, and 0.7 kg/h, it can be concluded that it has a higher PDP than the other model with 95 mm BFFSP. Therefore, it is safe to say that it may be more appropriate to choose a 95 mm BFFSP to achieve lower pressure loss and better performance.

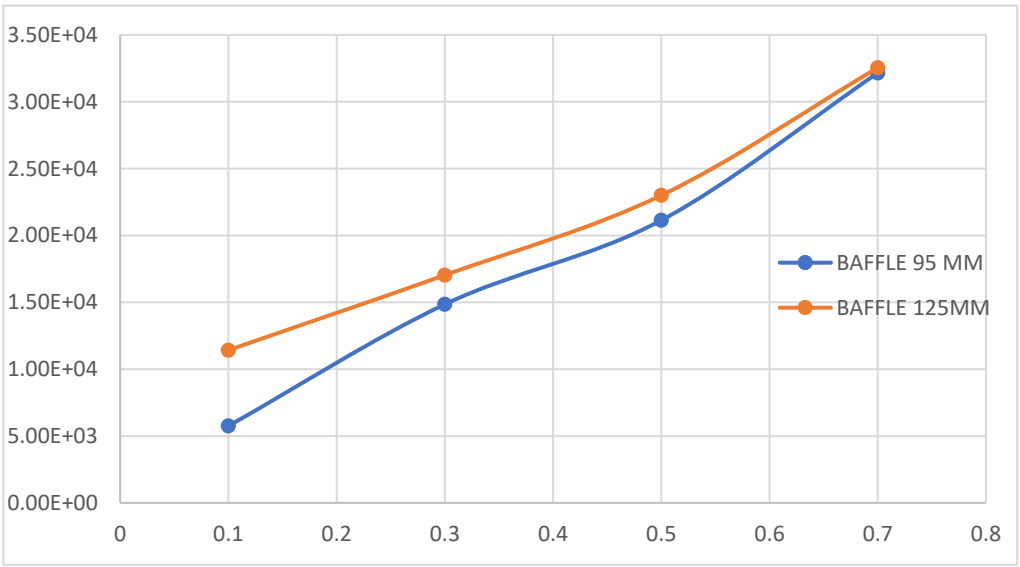

Figure 23. PDP for MFR at two baffle distances: 95 mm and 125 mm.

Figure 24 shows the relationship between HTRPD and MFRT. The effects of fluid behavior varying between two different baffle intervals of 95 mm and 125 mm can be defined by changes in MFRT on the HTRPD. Accordingly, it can be observed that HTRPD decreases accordingly when the MFRT increases to 0.1 kg/h, 0.3 kg/h, 0.5 kg/h, and 0.7 kg/h for all compartment spacings of the designed model, which are 95 mm and 125 mm. According to the conclusion drawn from Figure 24, in all cases where the MFRT of the model in geometry with 125 mm BFFSP is 0.1 kg/h, 0.3 kg/h, 0.5 kg/h, and 0.7 kg/h, it can be observed that it has a higher HTRPD than the other model with 95 mm BFFSP.

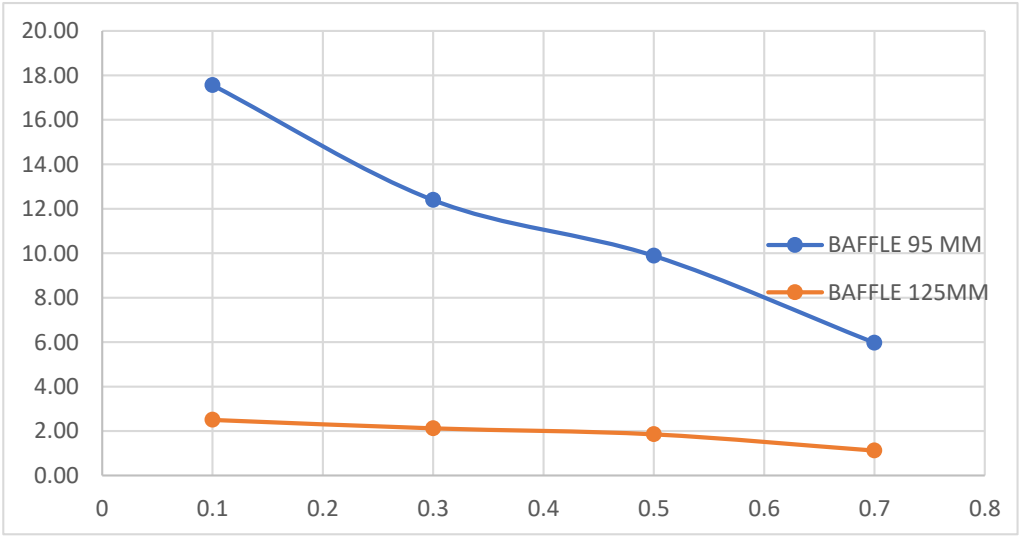

Figure 24. HTRPD for MFR at two baffle distances: 95 mm and 125 mm.

Simulation Results Analysis and Discussion: Effect of BFFSP on HEXR Performance

This study investigates the effect of BFFSP on HTCT and PDP in HEXRs. We examine the differences in fluid behavior with two different BFFSP configurations: 95 mm and 125 mm. Additionally, the impact of MFRT on the HEXR's output is explored.

Analysis of Results:

- **Higher BFFSP and Outlet Temperature:** For all MFRTs (0.1 kg/h, 0.3 kg/h, 0.5 kg/h, and 0.7 kg/h), the outlet temperature was consistently higher in the model with a 125 mm BFFSP compared to the 95 mm model. This suggests that the wider spacing might be hindering HTRFR, leading to a higher outlet temperature on the heated fluid side.
- **BFFSP and PDP:** The study found the opposite effect on PDP. In all MFR scenarios (0.1 kg/h, 0.3 kg/h, 0.5 kg/h, and 0.7 kg/h), the model with a 95 mm BFFSP exhibited a lower PDP compared to the model with a 125 mm gap. This indicates that the closer BFF arrangement promotes a more streamlined flow, resulting in a lower PDP across the HEXR.

Physical Discussion:

- **HTRFR:** The wider BFFSP might impede fluid mixing, reducing the HTRFR surface area. This can lead to a decrease in the HTCT and, consequently, a higher outlet temperature.
- **PDP:** Closer BFFs disrupt the fluid's flow path and increase turbulence, leading to pressure loss. This pressure loss translates to a higher energy requirement for the fluid to move forward. Therefore, a closer BFFSP results in a higher PDP.

In case 1, where the 120 mm SATHEC had a flow rate of 0.1 kg/s,
Re = 3024 was found.
In the second case, where the 120 mm SATHEC had a flow rate of 0.3 kg/s,
Re = 3678.58.
In the 3rd case, where the 120 mm SATHEC had a flow rate of 0.5 kg/s,

Re = 6048.05.

In the 4th case, where the 120 mm SATHEC had a flow rate of 0.7 kg/s, Re = 8420.58.

Calculated Reynolds numbers can be used to interpret the type and characteristics of the flow. Let us look at the type of flow in each case and what changes will be observed as the Reynolds number increases:

Case 1 (Flow: 0.1 kg/s, Re: 3024):

- Since the Reynolds number is greater than 2300, the flow is turbulent.
- Turbulent flow provides higher HTRFR and mixing.
- The PDP of the fluid is higher than in laminar flow.
- The risk of wear and corrosion on the pipe wall increases.

Case 2 (Flow: 0.3 kg/s, Re: 3678.58):

- The flow type is turbulent.
- Compared to case 1, the Reynolds number and therefore HTRFR, mixing, and PDP increase.

Case 3 (Flow: 0.5 kg/s, Re: 6048.05):

- The flow type is turbulent.
- Compared to the second case, the Reynolds number and other parameters increase further.

Case 4 (Flow: 0.7 kg/s, Re: 8420.58):

- The flow type is turbulent.
- In this case, the Reynolds number is quite high. At such a high Reynolds number, some changes in the behavior of the fluid can be observed:
- Turbulence becomes more intense.
- The risk of PDP and corrosion on the pipe wall increases.
- HTRFR and mixing are at levels close to maximum.

As the flow rate increases, the Reynolds number also increases. This means the flow becomes more turbulent. Turbulent flow increases HTRFR and mixing but also increases the risk of PDP and pipe wall corrosion. In practice, it is important to keep the Reynolds number at an optimum level for the desired result. Therefore, a comparative analysis of the results given here can be viewed in Table 2.

Table 2. Results of situations.

Baffle 95–125 mm Akış Hızı (Q)	Baffle 95 mm Re	Baffle 125 mm Re	Baffle 95 mm Nu	Baffle 125 mm Nu	Baffle 95 mm HTC (Predic.)	Baffle 95 mm HTC (Simulation)	Baffle 125 mm HTC (Predic.)	Baffle 125 mm HTC (Simulation)
0.1 kg/s	1739.13	1573.03	71.3	70.04	414.31 W/m^2K	453.89	371.75 W/m^2K	396.49
0.3 kg/s	5217.39	4719.09	83.4	82.13	492.03 W/m^2K	546.27	443.74 W/m^2K	485.24
0.5 kg/s	8695.65	7865.15	107.8	106.44	645.21 W/m^2K	693.43	576.14 W/m^2K	603.54
0.7 kg/s	12,173.91	10,911.21	132.2	130.75	798.39 W/m^2K	836.76	710.54 W/m^2K	746.91

First, Second, Third and Fourth Case Calculations as Body Material Aluminum and Tube Diameter 120 mm Calculation:

- Case 1 (Flow: 0.1 kg/s, Re: 3024):
- Pr = 6.21
- Nu (Dittus–Boelter) = 71.3
- Nu (Sieder–Tate) = 76.1
- Nu (Gnielinski) = 73.7
- Case 2 (Flow: 0.3 kg/s, Re: 3678.58):

Calculated in the same way, Nusselt numbers are found:

- Nu (Dittus–Boelter) = 83.4
- Nu (Sieder–Tate) = 88.4

- Nu (Gnielinski) = 86.0

○ Case 3 (Flow: 0.5 kg/s, Re: 6048.05):

Calculated in the same way, Nusselt numbers are found:

- Nu (Dittus–Boelter) = 107.8
- Nu (Sieder–Tate) = 113.3
- Nu (Gnielinski) = 110.6

○ Case 4 (Flow: 0.7 kg/s, Re: 8420.58):

Calculated in the same way, Nusselt numbers are found:

- Nu (Dittus–Boelter) = 132.2
- Nu (Sieder–Tate) = 138.1
- Nu (Gnielinski) = 134.7

The fact that the pipe material is aluminum significantly increases the Nusselt number and HTRFR. As the flow rate increases, the Nusselt number also increases. Dittus–Boelter, Sieder–Tate, and Gnielinski equations are valid for different ranges of Reynolds number and Prandtl number. Nusselt number is an important parameter in HTRFR and fluid mechanics. Nusselt number is used to calculate the HTCT.

Connection to the Context of the Paper:

This study emphasizes that BFFSP is a crucial factor in the design of HEXRs. By carefully considering the specific application and the desired balance between thermal performance and PDP, engineers can tailor the HEXR's configuration to maximize its effectiveness and contribute to both user savings and overall added value.

This study investigates the effect of BFFSP on HEXR output and highlights the importance of optimizing BFFSP. The work addresses the trade-off between HTRFR and PDP and provides insights to assist engineers in designing HEXRs.

Trade-off in the Context of the Research Paper:

In the context of the research paper, BFFSP presents a trade-off between HTRFR and PDP.

Wider BFFSP:

- May lead to slightly higher outlet temperatures: This is because the wider spacing might impede fluid mixing, reducing the HTRFR surface area.
- Has the advantage of lower PDPs: The wider spacing allows for a more streamlined flow, resulting in less disruption and pressure loss.

Closer BFFs:

- **Can offer better HTRFR:** The closer spacing promotes more turbulent flow and increases the HTRFR surface area, leading to more efficient HTRFR.
- **However, this comes at the cost of increased PDP:** The closer plates cause more disruption to the fluid flow, resulting in higher pressure loss.

Therefore, engineers must carefully consider the specific application and desired balance between thermal performance and PDP when designing HEXRs. They can tailor the BFFSP to optimize the HEXR's effectiveness and contribute to both user savings and overall added value.

This study investigates the impact of BFFSP on HEXR output. The analysis explores the trade-off between HTRFR yield and PDP for different baffle configurations (95 mm and 125 mm) and MFRTs (0.1 kg/s to 0.7 kg/s).

Wider BFFSP resulted in higher outlet temperatures, potentially due to reduced fluid mixing and HTRFR surface area. However, it also led to lower PDPs due to a more streamlined flow path. Conversely, closer BFFSP enhanced HTRFR by promoting turbulence and increasing the HTRFR area, but at the expense of higher PDP caused by flow disruption.

Reynolds number calculations confirm turbulent flow regimes for all scenarios. Nusselt number calculations (Dittus–Boelter, Sieder–Tate, Gnielinski) were performed considering the influence of pipe material (aluminum) and diameter (120 mm). The results

showcased a significant increase in Nusselt number and HTRFR due to aluminum compared to traditional materials.

This study emphasizes the importance of optimizing BFFSP in HEXR design. By understanding the trade-off between HTRFR and PDP, engineers can tailor baffle configurations for specific applications, maximizing effectiveness and contributing to overall value.

5. Conclusions

This study investigates the influence of BFFSP on the thermohydraulic output of SATHEC(s) using validated computational fluid dynamics (CFD) simulations. The effectiveness of CFD for HEXR design is established through comparisons with experimental data from Liu et al. [25] for various baffle configurations. The simulations demonstrate good agreement with the experiments, highlighting the potential of CFD for HEXR analysis. However, some discrepancies were observed, emphasizing the importance of BFF geometry in influencing flow patterns, pressure distribution, and temperature profiles within the HEXR. The study by Arani et al. examines HEXRs and how to optimize their designs for better output. It recognizes the balance between HTRFR and PDP in SATHEC and focuses on STHE. In the study, the effect of baffle design on HEXR output is analyzed. While analyzing it, it uses the computational fluid mechanics method, as we used in our study. The author's work focuses on STHE optimization with segmental deflectors with combined baffle and ribbed pipe configurations (triangular and circular). It compares the output of these configurations to a conventional STHE design. It analyzes the effect of different baffle and ribbed tube configurations on PDP, fluid flow path, and dead zones inside the HEXR. It introduces a new output evaluation criterion (PEC) that considers both HTRFR and PDP to determine the optimal configuration. In our own work, the Dittus–Boelter, Sieder–Tate and Gnielinski equations were used to calculate the Nusselt number. The results of the PDP that occurs when the fluid changes direction, as well as the HTRFR changes and PDPs that occur with baffle configurations, are similar to the results we found in our study [26].

In the study by Taher et al., five HEXRs with different deflection gaps were designed so that the helical deflection plates correspond to 40° helix angles. Designed partition gaps for case A: 15 mm (minimum selected area), for case B: P/16, for case C: P/8 (medium overlap type), and for case D: 3P/16 and E: P/4 (end-to-end type). P stands for helix pitch. As a result of the simulations, for the same MFRT, HTRFR per unit area decreases with increasing partition gaps just like in our study; however, for the same PDP, it is found that the largest baffle area (Case E) provides higher HTRFR and the pressure gradient also decreases with increasing baffle area [27]. Double-section baffles offer a significant advantage over their single-section counterparts, reducing PDP (ΔP) by a remarkable 70–75%. Helical baffles follow closely behind, achieving a 65–70% ΔP reduction compared to single-section designs. Conversely, the study highlights the inefficiency of three-piece partitions. Bloom BFFs emerge as another yield champion, boasting a 25–35% decrease in ΔP compared to traditional single-section baffles. Additionally, these innovative plates demonstrate a 30–35% reduction in bypass flow (U)—another factor contributing to improved output [28]. The research by He et al. delves deeper, employing the RNG k-ε model and standard wall treatment with boundary layers to create a comprehensive analysis. This study compares PDP and HTCTs of double-tube-pass SATHEC(s) (DTP-STHEs) equipped with different baffle configurations. Notably, the research introduces a novel and more effective method for evaluating STHE economic performance. Interestingly, the findings reveal that DTP-STHEs recover nearly double the heat compared to single-tube-pass exchangers while maintaining similar overall HTRFR rates. To gain a more nuanced understanding of thermohydraulic output in DTP-STHEs, researchers compared three configurations: segmental, helical, and flower baffles—all tested under identical conditions. The results expose a trade-off: flower baffles exhibit the lowest PDP but also the lowest HTCT. To provide a more holistic perspective on economic performance across these three configurations, the study introduces a new metric: HTRFR rate per effective pumping power (QH/P0). This combined measure promises a more balanced evaluation of yield gains. The simulation

results show that the QH/P0 of the flower baffle is the highest and the QH/P0 of the segmental baffle the lowest, and in our study, the optimized HEXR model, designed with a 95 mm BFFSP, offers a significant enhancement in HTRPD (up to 19.81%) compared to the wider 125 mm configuration. This translates to a potential increase in thermohydraulic output of up to 19.81% for the optimized design [29].

The study employs validated CFD simulations to explore the interplay between BFFSP, HTRFR yield, and PDP within the HEXR. Wider BFFSP (125 mm) consistently resulted in higher outlet temperatures for hot fluid across all investigated MFRTs (0.1 kg/h, 0.3 kg/h, 0.5 kg/h, and 0.7 kg/h). This indicates that a larger gap between baffles disrupts HTRFR from the hot fluid to the cold fluid, leading to a higher hot fluid outlet temperature. This finding highlights a potential drawback of wider spacing in applications where maximizing HTRFR is crucial.

Conversely, the PDP exhibited an opposite trend. The model with a narrower BFFSP (95 mm) consistently displayed a lower PDP compared to the 125 mm design at all flow rates. This can be attributed to the more streamlined flow path facilitated by the closer baffle arrangement. The reduced disruption by baffles minimizes the PDP experienced by the fluids within the HEXR. This suggests that a closer BFFSP configuration can be beneficial in applications prioritizing reduced pressure losses.

A key takeaway is the importance of considering the interplay between BFFSP, MFRT, and desired HEXR output. While wider spacing offers a slightly longer residency time for fluids, potentially increasing HTRFR, it comes at the cost of a higher PDP penalty. Conversely, a closer baffle arrangement promotes a more streamlined flow path, reducing PDP but potentially compromising HTRFR yield if the residence time becomes insufficient.

The findings demonstrate a clear correlation between BFFSP and thermohydraulic output. A decrease in PDP was observed with a closer spacing (95 mm) compared to a wider spacing (125 mm) across all flow rates. This aligns with the established principle that a more streamlined flow path reduces pressure losses within the HEXR. Consequently, a reduction in PDP contributes to an improvement in overall thermohydraulic output.

HTRPD serves as a valuable metric for evaluating the combined effects of HTRFR and PDP. The analysis revealed that the highest HTRPD values were achieved with the 95 mm BFFSP configuration, particularly at the lowest MFRT (0.1 kg/h). This suggests that the optimized HEXR model, designed with a 95 mm BFFSP, offers a significant enhancement in HTRPD (up to 19.81%) compared to the wider 125 mm configuration. This translates to a potential increase in thermohydraulic output of up to 19.81% for the optimized design.

This study emphasizes the importance of optimizing BFFSP during HEXR design. By carefully considering the specific application requirements, engineers can determine the targeted balance between thermal performance and PDP. For instance, maximizing HTRFR might favor wider spacing despite the increased PDP, while minimizing pressure losses might prioritize closer spacing, even if it sacrifices some HTRFR yield.

Optimizing BFFSP during HEXR design can lead to significant benefits in various industrial applications. It can contribute to improved overall HEXR yield by achieving the desired HTRFR rate while minimizing pressure losses. This translates to reduced operational costs associated with pumping power requirements and potentially a more compact HEXR design if a higher HTRFR rate can be achieved with a smaller unit due to a strategically chosen BFFSP.

Author Contributions: Conceptualization, M.A.K. and A.F.; methodology, M.A.K.; software, M.A.K.; validation, M.A.K.; formal analysis, M.A.K.; investigation, M.A.K.; resources, M.A.K.; data curation, M.A.K.; writing—original draft, M.A.K.; writing—review & editing, M.A.K.; visualization, M.A.K.; supervision, M.A.K.; project administration, M.A.K.; funding acquisition, M.A.K. and A.F. All authors have read and agreed to the published version of the manuscript.

Funding: This research received no external funding.

Data Availability Statement: Not applicable.

Conflicts of Interest: The authors declare no conflicts of interest.

Nomenclature

SATHEC(s)	Shell-and-tube heat exchanger(s)
HEXR(s)	Heat exchanger(s)
HTCT	Heat transfer coefficient
MFRT	Mass flow rate
HTRPD	Heat transfer rate per pressure drop
PDP	Pressure drop
BFF	Baffle plate
BFFSP	Baffle spacing
HTRFR	Heat transfer
RKEM	The realizable k-ε turbulence model
T:	Temperature (K)
C	Capacity ratio
ΔP	Pressure drop (Pa)
N	Number of shell passes
c_p	Specific heat capacity ($J \cdot kg^{-1} \cdot K^{-1}$)
ρ	Density
u	Velocity in x-direction (m/s)
v	Velocity in y-direction (m/s)
w	Velocity in z-direction (m/s)
t	Time (s)
p	Pressure (Pa)
μ	Dynamic viscosity (Pa·s)
k	Turbulent kinetic energy (m^2/s^2)
ε	Turbulent energy dissipation rate (m^2/s^3)
Γ	Production term for turbulent kinetic energy (dimensions depend on context)

References

1. Kern, D.Q. *Process Heat Transfer*; McGraw-Hill: New York, NY, USA, 1950.
2. Bell, K.J. Delaware method for shell side design. In *Heat Exchangers: Thermal–Hydraulic Fundamentals and Design*; Kakaç, S., Bergles, A.E., Mayinger, F., Eds.; Hemisphere: New York, NY, USA, 1981; pp. 581–618.
3. Gay, B.; Mackley, N.; Jenkins, J. Shell-side heat transfer in baffled cylindrical shell- and tube exchangers—An electrochemical mass-transfer modelling technique. *Int. J. Heat Mass Transf.* **1976**, *19*, 995–1002. [CrossRef]
4. Halle, H.; Chenoweth, J.M.; Wabsganss, M.W. Shell side water flow pressure drop distribution measurements in an industrial-sized test heat exchanger. *J Heat Transf.* **1988**, *110*, 60–67. [CrossRef]
5. Pekdemir, T.; Davies, T.W.; Haseler, L.E.; Diaper, A.D. Pressure drop measurements on the shell side of a cylindrical shell-and-tube heat exchanger. *Heat Transf. Eng.* **1994**, *15*, 42–56. [CrossRef]
6. Gaddis, E.S.; Gnielinski, V. Pressure drop on the shell side of shell-and-tube heat exchangers with segmental baffles. *Chem. Eng. Process.* **1997**, *36*, 149–159. [CrossRef]
7. Karno, A.; Ajib, S. Effect of tube pitch on heat transfer in shell-and-tube heat exchangers—New simulation software. *Heat Mass Transf.* **2006**, *42*, 263–270. [CrossRef]
8. Prithiviraj, M.; Andrews, M.J. Three dimensional numerical simulation of shell-and-tube heat exchangers. Part 1: Foundation and Fluid Mechanics. *Numer. Heat Transf. Part A Appl.* **1998**, *33*, 817–828. [CrossRef]
9. Stevanović, Ž; Ilić, G.; Radojković, N.; Vukić, M.; Stefanović, V.; Vučković, G. Design of shell and tube heat exchangers by using CFD technique—Part one: Thermo hydraulic calculation. *Facta Univ. Ser. Mech. Eng.* **2001**, *8*, 1091–1105.
10. Kapale, U.C.; Chand, S. Modeling for shell-side pressure drop for liquid flow in shell-and-tube heat exchanger. *Int. J. Heat Mass Transf.* **2006**, *49*, 601–610. [CrossRef]
11. Sparrow, E.; Reifschneider, L. Effect of interbaffle spacing on heat transfer and pressure drop in a shell-and-tube heat exchanger. *Int. J. Heat Mass Transf.* **1986**, *29*, 1617–1628. [CrossRef]
12. Ji, J.; Lu, Y.; Shi, B.; Gao, R.; Chen, Q. Numerical research on vibration and heat transfer performance of a conical spiral elastic bundle heat exchanger with baffles. *Appl. Therm. Eng.* **2023**, *232*, 121036. [CrossRef]
13. Tandiroglu, A. Effect of flow geometry parameters on transient heat transfer for turbulent flow in a circular tube with baffle inserts. *Int. J. Heat Mass Transf.* **2006**, *49*, 1559–1567. [CrossRef]
14. Jayranaiwachira, N.; Promvonge, P.; Thianpong, C.; Skullong, S. Entropy generation and thermal performance of tubular heat exchanger fitted with louvered corner-curved V-baffles. *Int. J. Heat Mass Transf.* **2023**, *201*, 123638. [CrossRef]
15. Li, L.; Xu, W.; Tan, Y.; Yang, Y.; Yang, J.; Tan, D. Fluid-induced vibration evolution mechanism of multiphase free sink vortex and the multi-source vibration sensing method. *Mech. Syst. Signal Process.* **2023**, *189*, 110058. [CrossRef]

16. Li, L.; Li, Q.; Ni, Y.; Wang, C.; Tan, Y.; Tan, D. Critical penetrating vibration evolution behaviors of the gas-liquid coupled vortex flow. *Energy* **2024**, *292*, 130236. [CrossRef]
17. Abdollahpour, M.S.; Darbandi, M. Developing an algorithm to evaluate the tube and baffle choice influences on enhancing the hydrothermal performances of shell and tube heat exchangers. *Int. J. Heat Mass Transf.* **2024**, *222*, 125178. [CrossRef]
18. Al-Darraji, A.R.; Marzouk, S.; Aljabr, A.; Almehmadi, F.A.; Alqaed, S.; Kaood, A. Enhancement of heat transfer in a vertical shell and tube heat exchanger using air injection and new baffles: Experimental and numerical approach. *Appl. Therm. Eng.* **2024**, *236 Pt A*, 121493. [CrossRef]
19. Abdelmoety, A.M.; Muhieldeen, M.W.; Tey, W.Y.; Yin, X.; Beit, N.E. Numerical investigations on optimised shell designs of a U-tube heat exchanger. *Therm. Sci. Eng. Prog.* **2024**, *47*, 102327. [CrossRef]
20. El-Said, E.M.; Abou Al-Sood, M.M. Shell and tube heat exchanger with new segmental baffles configurations: A comparative experimental investigation. *Appl. Therm. Eng.* **2019**, *150*, 803–810. [CrossRef]
21. Cabello, R.; Popescu, A.E.P.; Bonet-Ruiz, J.; Cantarell, D.C.; Llorens, J. Heat transfer in pipes with twisted tapes: CFD simulations and validation. *Comput. Chem. Eng.* **2022**, *166*, 107971. [CrossRef]
22. Liu, X.; Fu, Y.; Wang, J.; Zhang, H.; Zhu, J. Investigation on flow and heat transfer in rectangular cross-section sinusoidal channels. *Int. J. Therm. Sci.* **2022**, *176*, 107490. [CrossRef]
23. Mukherjee, R. Effectively design shell-and-tube heat exchangers. *Chem. Eng. Prog.* **1998**, *94*, 21–37.
24. Gaddis, E.S.; Gnielinski, V. Shell-side heat transfer in baffled shell-and-tube heat exchangers. In *VDI-Heat Atlas*; VDI-Verlag: Düsseldorf, Germany, 1993; pp. 1–5.
25. Cao, X.; Chen, D.; Du, T.; Liu, Z.; Ji, S. Numerical investigation and experimental validation of thermo-hydraulic and thermodynamic performances of helical baffle heat exchangers with different baffle configurations. *Int. J. Heat Mass Transf.* **2020**, *160*, 120181. [CrossRef]
26. Arani, A.A.A.; Moradi, R. Shell and tube heat exchanger optimization using new baffle and tube configuration. *Appl. Therm. Eng.* **2019**, *157*, 113736. [CrossRef]
27. Taher, F.N.; Movassag, S.Z.; Razmi, K.; Azar, R.T. Baffle space impact on the performance of helical baffle shell and tube heat exchangers. *Appl. Therm. Eng.* **2012**, *44*, 143–149. [CrossRef]
28. Ambekar, A.S.; Sivakumar, R.; Anantharaman, N.; Vivekenandan, M. CFD simulation study of shell and tube heat exchangers with different baffle segment configurations. *Appl. Therm. Eng.* **2016**, *108*, 999–1007. [CrossRef]
29. He, L.; Li, P. Numerical investigation on double tube-pass shell-and-tube heat exchangers with different baffle configurations. *Appl. Therm. Eng.* **2018**, *143*, 561–569. [CrossRef]

Disclaimer/Publisher's Note: The statements, opinions and data contained in all publications are solely those of the individual author(s) and contributor(s) and not of MDPI and/or the editor(s). MDPI and/or the editor(s) disclaim responsibility for any injury to people or property resulting from any ideas, methods, instructions or products referred to in the content.